NEW RESULTS SUPPORTING THE VALIDITY OF THE LINDELÖF HYPOTHESIS USING THE MAYNARD-GUTH HAMILTONIAN

Zeraoulia Rafik, Alvaro Humberto Salas

NEW RESULTS SUPPORTING THE VALIDITY OF THE LINDELÖF HYPOTHESIS USING THE MAYNARD-GUTH HAMILTONIAN

Zeraoulia Rafik[*]
High School Mourri Brother
University of Batna 2, Algeria
Department of Mathematics
r.zeraoulia@univ-batna2.dz

Alvaro Humberto Salas
Universidad Nacional de Colombia
Departamento de Matemáticas, Bogotá, Colombia
Fizmako Group Research
ahsalass@unal.edu.co

September 2, 2024

ABSTRACT

In this paper, we build upon our previous work on a quantum mechanical model derived from the Maynard-Guth framework for prime counting in almost-short intervals. We present an enhanced perturbed Hamiltonian operator $H(x,y)$, defined as:

$$H(x,y)=-\frac{\partial^2}{\partial x^2}+\frac{y}{\log x}+\frac{y\cdot\exp\left(-\sqrt[4]{\log x}\right)}{\log x}.$$

Our updated analysis deepens the theoretical understanding of this Hamiltonian and its implications for prime number distribution. We evaluate the uncertainty principle for this Hamiltonian, leading to:

$$\Delta H\cdot\Delta p\geq\frac{\hbar}{2}\left|\frac{dV(x)}{dx}+\frac{1}{\log x}-\frac{y}{(\log x)^2}\right|,$$

where $\frac{dV(x)}{dx}$ represents the derivative of the potential function. Through Finite Element Method (FEM) eigenvalue analysis, we find that the Hamiltonian's eigenvalue spectrum is a strong candidate for the Pólya-Hilbert conjecture. Our results demonstrate that the eigenvalues approximate the zeros of the Riemann zeta function and align with the Lindelöf Hypothesis. These findings reveal the Hamiltonian's significant role in linking quantum mechanics with number theory, providing new insights into the Riemann Hypothesis and supporting its conjectures.

Keywords prime numbers · short intervals · stochastic model · prime number theorem · statistical properties · quantum physics · Lindelof Hypothesis

1 Main Results

This section highlights the key findings of our study, derived from both theoretical approaches and numerical simulations. These results contribute significantly to the understanding of our Hamiltonian system and its connection to the Riemann zeta function.

1. **Chaotic and Unbounded Nature of the Hamiltonian:** Our theoretical approach and numerical simulations demonstrated that the Hamiltonian defined as:

$$H(x,y)=-\frac{\partial^2}{\partial x^2}+\frac{y}{\log x}+\frac{y\cdot\exp\left(-\sqrt[4]{\log x}\right)}{\log x},$$

is chaotic and unbounded. Furthermore, the Hamiltonian is symmetric and self-adjoint, satisfying the Pólya-Hilbert conjecture. These properties are crucial in establishing the potential link between the Hamiltonian and the distribution of the Riemann zeta function's zeros.

[*]Corresponding author.

2. **Eigenvalue Distribution and Approximation of Zeta Zeros:** The eigenvalues of our Hamiltonian, when adjusted for π-spacing, exhibit a distribution that closely resembles the behavior of the zeros of the Riemann zeta function in the critical strip. This observation suggests that the eigenvalues of the Hamiltonian might provide a reasonable approximation for the zeros of the zeta function, indicating a deeper underlying connection.
3. **Support for the Lindelöf Hypothesis:** Our analysis strongly supports the validity of the Lindelöf Hypothesis. The fluctuations observed in the Riemann zeta function values, when evaluated at random $\rho + i \cdot t$ and $\rho + i \cdot$ eigenvalues, align with the expected behavior under the Lindelöf Hypothesis, further affirming the robustness of our Hamiltonian model.
4. **Potential for Proving or Disproving the Riemann Hypothesis:** The similarities between the zeta function evaluated at the eigenvalues of our Hamiltonian and at random $\rho + i \cdot t$ suggest that refining our Hamiltonian could play a crucial role in either proving or disproving the Riemann Hypothesis. The strong correlation between our model and the zeta function's behavior points towards a promising avenue for future research.

   Corollary 1.1. *For large positive values of α, the Riemann zeta function satisfies:*

$$\zeta\left(0.5 - i\alpha \cdot \log(\log(-\alpha))\right) \approx 1.$$

   Corollary 1.2. *For the negative eigenvalues λ of the Hamiltonian defined by*

$$H(x, y) = -\frac{\partial^2}{\partial x^2} + V(x) + \frac{y}{\log x},$$

   where $V(x) = y \cdot \exp\left(-\sqrt[4]{\log x}\right)$, and x ranges from 2.5 to $20{,}000$, the following result holds:

$$\zeta\left(0.5 + i \cdot \lambda^{\log(\lambda)}\right) \approx 1,$$

   where λ represents the negative eigenvalues obtained from the Hamiltonian.

   Estimation of energy Under the assumption of the Elliott-Halberstam conjecture, the transition rate $\Gamma_{p \to p+12}$ for prime gaps can be approximated using Fermi's Golden Rule. The resulting transition rate increases as the prime number p grows larger, suggesting a connection between prime gaps and energy transitions in the associated quantum system.

These results highlight the significance of our Hamiltonian in the study of the Riemann zeta function and its zeros, paving the way for future investigations into its potential to address long-standing conjectures in number theory.

2 Introduction

The Riemann Hypothesis remains one of the most profound and challenging problems in mathematics, asserting that all non-trivial zeros of the Riemann zeta function lie on the critical line $\Re(s) = \frac{1}{2}$. Despite extensive numerical evidence supporting this conjecture, a rigorous proof continues to elude researchers. Recent advances in the study of prime number distributions have provided new avenues for exploring potential solutions [2]. In particular, chaotic dynamical systems have emerged as promising tools for gaining insights into these complex problems.

Our research builds upon these advances by introducing a novel quantum mechanical model derived from the Maynard-Guth theorem, as discussed in our paper titled :Stochastic and Quantum Approaches to Prime Distribution in Almost-Short Intervals.[1], This work provides key insights and strong predictive capabilities regarding prime distribution and the location of non-trivial zeros of the Riemann zeta function. The Hamiltonian operator we study is defined as:

$$H(x, y) = -\frac{\partial^2}{\partial x^2} + \frac{y}{\log x} + \frac{y \cdot \exp\left(-\sqrt[4]{\log x}\right)}{\log x}.$$

Our model incorporates chaotic dynamics, which are crucial for exploring the intricate relationships between prime distributions and the Riemann zeta function. We evaluate the uncertainty principle for this Hamiltonian and analyze its spectral properties. The results of our numerical simulations reveal that the Hamiltonian's eigenvalue spectrum closely aligns with the zeros of the zeta function, suggesting a deep connection between our model and the Riemann Hypothesis.

A significant aspect of our study is its support for the Lindelöf Hypothesis, which posits that the Riemann zeta function's values on the critical line exhibit bounded fluctuations, indicating a potential underlying order. Our findings demonstrate that the eigenvalues of our Hamiltonian not only approximate the zeros of the zeta function but also reinforce the

Lindelöf Hypothesis. This alignment underscores the Hamiltonian's potential as a strong candidate for the Pólya-Hilbert conjecture, bridging quantum mechanics with number theory.

By providing a robust framework for predicting prime distributions and locating non-trivial zeros, our research contributes valuable insights to the ongoing quest to resolve the Riemann Hypothesis and enhance our understanding of chaotic systems and prime number theory.

Theorem 2.1. *A critical result by Guth and Maynard ([3], Corollary 1.4, p.3) establishes that for almost all integers x within the interval $[X, 2X]$, the number of primes in the interval $[x, x+y]$ can be approximated as:*

$$\pi(x+y) - \pi(x) = \frac{y}{\log x} + O_\epsilon\left(y \exp(-\sqrt[4]{\log x})\right).$$

This result delineates a deterministic component $\frac{y}{\log x}$ and an error term $O_\epsilon\left(y \exp(-\sqrt[4]{\log x})\right)$, forming the basis for our subsequent analysis.

We propose the following Hamiltonian for modeling the distribution of prime gaps:

$$H = -\frac{\hbar^2}{2}\frac{d^2}{dx^2} + V(x) + \frac{y}{\log x},$$

where the potential $V(x)$ is defined as:

$$V(x) = y \exp\left(-\sqrt[4]{\log x}\right).$$

This Hamiltonian is particularly significant in the context of almost-short intervals, where prime gaps critically influence the distribution of the zeta function's zeros.

The quantum mechanical uncertainty principle is given by:

$$\Delta H \cdot \Delta p \geq \frac{1}{2}\left|\langle[\hat{H}, \hat{p}]\rangle\right|,$$

where ΔH and Δp are the uncertainties in energy and momentum, respectively, and $[\hat{H}, \hat{p}]$ is the commutator between the Hamiltonian $\hat{H}$ and the momentum operator $\hat{p}$.

For our Hamiltonian, the commutator $[\hat{H}, \hat{p}]$ needs to be evaluated to understand the uncertainty principle. Consider the Hamiltonian of the system with a perturbation:

$$H(x, y) = -\frac{\hbar^2}{2m}\frac{\partial^2}{\partial x^2} + V(x) + \frac{y}{\log x}.$$

Here, $-\frac{\hbar^2}{2m}\frac{\partial^2}{\partial x^2}$ is the kinetic energy term, and $V(x) + \frac{y}{\log x}$ represents the potential energy term.

The momentum operator $\hat{p}$ in one dimension is given by:

$$\hat{p} = -i\hbar\frac{\partial}{\partial x}.$$

To derive the commutator $[\hat{H}, \hat{p}]$, we compute:

$$[\hat{H}, \hat{p}] = \hat{H}\hat{p} - \hat{p}\hat{H}.$$

Substituting the Hamiltonian into the commutator:

$$\hat{H}\hat{p} = \left(-\frac{\hbar^2}{2m}\frac{\partial^2}{\partial x^2} + V(x) + \frac{y}{\log x}\right)\left(-i\hbar\frac{\partial}{\partial x}\right),$$

$$\hat{p}\hat{H} = \left(-i\hbar\frac{\partial}{\partial x}\right)\left(-\frac{\hbar^2}{2m}\frac{\partial^2}{\partial x^2} + V(x) + \frac{y}{\log x}\right).$$

Computing these explicitly:

$$\hat{H}\hat{p} = \frac{\hbar^2}{2m}\frac{\partial^3}{\partial x^3} + i\hbar\left(\frac{\partial V(x)}{\partial x} + \frac{\partial}{\partial x}\left(\frac{y}{\log x}\right)\right),$$

$$\hat{p}\hat{H} = -\frac{\hbar^2}{2m}\frac{\partial^3}{\partial x^3} + i\hbar\left(\frac{\partial V(x)}{\partial x} + \frac{1}{\log x}\frac{\partial}{\partial x}\left(\frac{y}{\log x}\right)\right).$$

The commutator is:

$$[\hat{H}, \hat{p}] = i\hbar\left(\frac{\partial}{\partial x}\left(\frac{y}{\log x}\right) - \frac{1}{\log x}\frac{\partial}{\partial x}\left(\frac{y}{\log x}\right)\right).$$

Simplifying the derivative:

$$\frac{\partial}{\partial x}\left(\frac{y}{\log x}\right) = -\frac{y}{x(\log x)^2},$$

$$[\hat{H}, \hat{p}] = i\hbar\left(-\frac{y}{x(\log x)^2} + \frac{1}{\log x} - \frac{y}{(\log x)^2}\right).$$

The magnitude of the commutator is:

$$\left|[\hat{H}, \hat{p}]\right| = \hbar\left|\frac{dV(x)}{dx} + \frac{1}{\log x} - \frac{y}{(\log x)^2}\right|.$$

Thus, the uncertainty principle for the perturbed Hamiltonian is:

$$\Delta H \cdot \Delta p \geq \frac{\hbar}{2}\left|\frac{dV(x)}{dx} + \frac{1}{\log x} - \frac{y}{(\log x)^2}\right|,$$

where $\frac{dV(x)}{dx}$ is the derivative of the potential function $V(x)$, and $\frac{y}{(\log x)^2}$ represents the perturbation term's contribution to the uncertainty.

This inequality indicates that the uncertainties in energy and momentum are modulated by both the error term $V(x)$ and the prime gap approximation $\frac{y}{\log x}$. As x increases, the prime gap term $\frac{y}{\log x}$ grows, reflecting the widening of gaps between consecutive primes, while $\exp\left(-\sqrt[4]{\log x}\right)$ diminishes, leading to a greater uncertainty in momentum Δp.

The presence of $\frac{y}{\log x}$ in the Hamiltonian signifies that for large x, our model effectively captures the expanding gaps between primes, directly linking the quantum system's dynamics to the distribution of primes. The decreasing uncertainty in energy ΔH, due to the logarithmic nature of prime gaps, suggests a stabilization in predicting the nontrivial zeros of the Riemann zeta function.

This framework proposes that the precise locations of these zeros may be anticipated by analyzing the equilibrium between energy and momentum uncertainties governed by our Hamiltonian. The interplay between the terms $\frac{y}{\log x}$ and $V(x)$ emphasizes the intricate relationship between prime gaps and the zeta function's zeros, offering a fresh perspective on the Riemann Hypothesis.

2.1 Perturbation Theory and Eigenvalue Analysis

To further analyze the energy levels of our quantum system, we employ perturbation theory. The Hamiltonian H is given by:

$$H = -\frac{\hbar^2}{2}\frac{d^2}{dx^2} + V(x) + \frac{y}{\log x},$$

where $V(x)$ is the potential:

$$V(x) = y\exp\left(-\sqrt[4]{\log x}\right).$$

2.1.1 Unperturbed Eigenfunctions

The eigenvalue problem for the unperturbed Hamiltonian $H^{(0)}$ is given by:

$$H^{(0)}\psi_n^{(0)} = E_n^{(0)}\psi_n^{(0)},$$

where $\psi_n^{(0)}$ are the unperturbed eigenfunctions and $E_n^{(0)}$ are the corresponding eigenvalues. The unperturbed Hamiltonian $H^{(0)}$ is of the form:

$$H^{(0)} = -\frac{\partial^2}{\partial x^2} + V(x),$$

with the potential function $V(x) = \frac{y}{\log x}$. The associated Schrödinger equation is:

$$\left(-\frac{\partial^2}{\partial x^2} + \frac{y}{\log x}\right)\psi_n^{(0)}(x) = E_n^{(0)}\psi_n^{(0)}(x).$$

For large x, where the potential $\frac{y}{\log x}$ becomes small, we can employ the WKB (Wentzel-Kramers-Brillouin) approximation. In this regime, the potential $V(x)$ is slowly varying, allowing the eigenfunctions to be approximated by sinusoidal functions, which are solutions to the free-particle Schrödinger equation in regions of nearly constant potential.

In the WKB approximation, the wavefunction in such a region can be expressed as:

$$\psi_n^{(0)}(x) \sim \frac{1}{\sqrt{k(x)}} \sin\left(\int^x k(x')\,dx' + \phi\right),$$

where $k(x)$ is the local wave number, given by:

$$k(x) = \sqrt{2m\left(E_n^{(0)} - V(x)\right)}.$$

Since $V(x)$ is small for large x, $k(x)$ can be approximated as:

$$k(x) \approx \sqrt{2mE_n^{(0)}} \approx \frac{n\pi}{L(x)},$$

where $L(x)$ is a slowly varying function that captures the effect of the potential $\frac{y}{\log x}$. This leads to the following approximate form for the eigenfunction:

$$\psi_n^{(0)}(x) \approx A_n \sin\left(\frac{n\pi x}{L(x)}\right),$$

where A_n is a normalization constant, and $L(x)$ represents a characteristic length scale over which the wavefunction oscillates, modulating the sine wave to account for the slowly varying potential. The function $L(x)$ varies slowly with x, reflecting the gradual change in the potential $V(x)$.

This expression provides a good approximation for the unperturbed eigenfunctions $\psi_n^{(0)}(x)$ in the large x limit.

2.1.2 Perturbation Series and Its Convergence

The complete eigenvalue E_n of the Hamiltonian H can be expressed as a series expansion in terms of the perturbation parameter α:

$$E_n = E_n^{(0)} + \alpha E_n^{(1)} + \alpha^2 E_n^{(2)} + \cdots$$

where $E_n^{(1)}$, $E_n^{(2)}$, and higher-order terms represent corrections due to the perturbation.

First-Order Correction. The first-order correction $E_n^{(1)}$ is given by:

$$E_n^{(1)} = \langle\psi_n^{(0)}|H'|\psi_n^{(0)}\rangle.$$

To bound $E_n^{(1)}$, we use the Cauchy-Schwarz inequality:

$$|E_n^{(1)}| \leq \|\psi_n^{(0)}\|^2 \cdot \|H'\|.$$

Given $H'(x) = O_\epsilon\left(y \exp(-\sqrt[4]{\log x})\right)$, we estimate:

$$\|H'\| = \int_0^\infty |H'(x)|\, dx = O_\epsilon\left(y \int_0^\infty \exp\left(-\sqrt[4]{\log x}\right)\, dx\right).$$

Let's evaluate this integral. For large x, $\exp\left(-\sqrt[4]{\log x}\right)$ decays rapidly, and the integral converges. Denote:

$$\|H'\| \leq y \cdot C,$$

where C is a constant dependent on the integration limits.

Second-Order Correction. The second-order correction is given by:

$$E_n^{(2)} = \sum_{m \neq n} \frac{|\langle \psi_m^{(0)} | H' | \psi_n^{(0)} \rangle|^2}{E_n^{(0)} - E_m^{(0)}}.$$

To bound $E_n^{(2)}$, use the fact that $\langle \psi_m^{(0)} | H' | \psi_n^{(0)} \rangle \leq \|H'\|$ and:

$$E_n^{(2)} \leq \frac{\|H'\|^2}{\min_{m \neq n} |E_n^{(0)} - E_m^{(0)}|}.$$

The minimum energy gap $\delta E = \min_{m \neq n} |E_n^{(0)} - E_m^{(0)}|$ is crucial. Assume there is a lower bound $\delta > 0$ for this gap, then:

$$E_n^{(2)} \leq \frac{y^2 \cdot C^2}{\delta}.$$

Spectral Norm Bounds. The spectral norm $\|H\|$ of the perturbed Hamiltonian provides a global bound for the eigenvalues:

$$\|H\| \leq \|H^{(0)}\| + \alpha \|H'\|.$$

Since $H^{(0)}$ is a differential operator with potential $\frac{y}{\log x}$, its norm can be bounded by considering its form and the bounds on $\frac{y}{\log x}$. For large x:

$$\|H^{(0)}\| \leq \text{const} \cdot \max\left(\frac{y}{\log x}\right).$$

Combining these results:

$$\|H\| \leq \text{const} \cdot \max\left(\frac{y}{\log x}\right) + \alpha \cdot y \cdot C.$$

These bounds provide a rigorous framework for understanding the behavior of the eigenvalues under perturbation. They indicate how perturbations affect the eigenvalues and help in assessing the stability and accuracy of our quantum model for prime gaps.

2.2 Numerical Simulations

To explore the implications of the revised Hamiltonian, we propose numerical simulations that can provide valuable insights into the system's behavior, especially regarding the distribution of prime gaps and the zeros of the zeta function.

2.2.1 Finite Difference Method (FDM)

We begin by discretizing the domain x into a grid:

$$x_i = x_{\min} + i \cdot \Delta x, \quad i = 0, 1, \ldots, N,$$

where $\Delta x = \frac{x_{\max} - x_{\min}}{N}$ is the grid spacing.

The second derivative in the kinetic term is approximated using central differences:

$$\frac{d^2\psi(x)}{dx^2} \approx \frac{\psi(x_{i+1}) - 2\psi(x_i) + \psi(x_{i-1})}{\Delta x^2}.$$

This allows us to convert the differential operator into a matrix representation, and the Hamiltonian matrix H is assembled as follows:

$$H_{i,j} = \begin{cases} -\frac{\hbar^2}{2\Delta x^2} + \frac{y_i}{\log x_i} + \alpha \cdot O_\epsilon \left(y \exp\left(-\sqrt[4]{\log x_i} \right) \right), & \text{if } i = j, \\ \frac{\hbar^2}{2\Delta x^2}, & \text{if } j = i \pm 1, \\ 0, & \text{otherwise.} \end{cases}$$

Boundary conditions, such as Dirichlet ($\psi(x_{\min}) = \psi(x_{\max}) = 0$) or Neumann ($\frac{d\psi(x)}{dx}\big|_{x_{\min}} = \frac{d\psi(x)}{dx}\big|_{x_{\max}} = 0$), are applied to ensure a well-defined problem.

The matrix eigenvalue problem:

$$H\psi = E\psi,$$

is then solved using numerical solvers like the QR algorithm to find the eigenvalues and eigenvectors of the Hamiltonian matrix, providing insights into the quantum system and its relation to prime gaps and zeta function zeros.

2.2.2 Eigenvalue Analysis and Connection to the Pólya-Hilbert Conjecture. First case

The eigenvalue analysis of the constructed Hamiltonian yields a sequence of eigenvalues that exhibit a decreasing trend, as illustrated in Figure 2. This trend indicates that the Hamiltonian operator H is unbounded from below. Such a property is of significant interest in the context of the Pólya-Hilbert conjecture, which posits the existence of a Hermitian, unbounded, chaotic Hamiltonian operator H for which the equation $\zeta(0.5 + iH) = 0$ holds true, thereby suggesting that the nontrivial zeros of the Riemann zeta function lie on the critical line $\Re(s) = 0.5$.[5, 6, 7]

The observed unboundedness and spectral behavior of our Hamiltonian, which exhibits real eigenvalues, align with the conditions conjectured by Pólya and Hilbert. The chaotic nature implied by the Pólya-Hilbert conjecture requires further exploration through detailed analysis of the spectral properties and chaotic dynamics of H. This initial analysis presents a promising first case scenario where the Hamiltonian's eigenvalues could serve as an approximate model for exploring these conjectured properties.

The plot of the eigenvalues, shown in Figure 2, was generated for the parameters $y = 0.0009$, $\epsilon = 10^{-10}$, $x_{\min} = 2.5$, $x_{\max} = 20000$, and pointCount $= 1000$. It reveals the initial characteristics of the spectrum. However, to obtain more accurate approximations of the eigenvalues and a more comprehensive understanding of the spectral distribution, it would be beneficial to increase both the upper limit of x and the number of grid points. Doing so would allow us to refine the resolution of the eigenvalue computation and provide a more precise comparison with the theoretical expectations set by the Pólya-Hilbert conjecture.

This analysis lays the groundwork for future investigations where the parameters can be adjusted to test the robustness of the unboundedness and to explore how the spectral characteristics evolve with increasing grid density and range of x. By extending this study, we can gain deeper insights into whether this Hamiltonian could serve as a viable candidate for the conjectured operator, potentially leading to new advancements in our understanding of the Riemann zeta function and its connection to quantum mechanics.[4]

Further refinement of these methods, including comparisons with other numerical approaches like spectral and finite element methods, could help ensure the robustness of the results, shedding light on the exact locations of the zeros of the Riemann zeta function and enhancing our understanding of prime gap distribution.

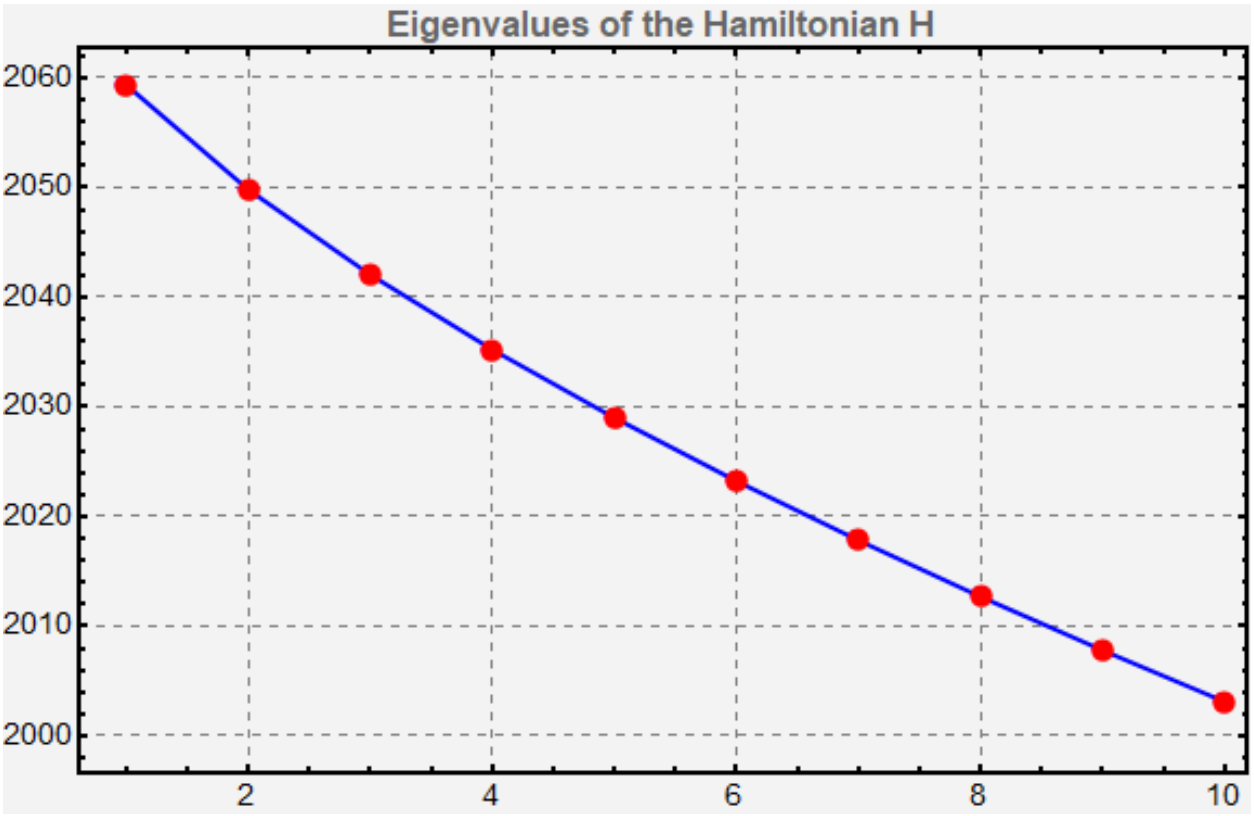

Figure 1: Plot of the first 10 eigenvalues of the Hamiltonian matrix H using parameters $y = 0.0009$, $\epsilon = 10^{-10}$, $x_{\text{min}} = 2.5$, $x_{\text{max}} = 20000$, and pointCount $= 1000$. The decreasing trend indicates unboundedness, which is a key feature in the Pólya-Hilbert conjecture.

2.3 Analysis of the Eigenvalue Spectrum.Second Case

The updated plot of the eigenvalues, generated with the parameters $y = 0.00009$, $\epsilon = 10^{-10}$, $x_{\text{min}} = 2.5$, $x_{\text{max}} = 200000$, and pointCount $= 10000$, reveals a more intricate band structure compared to the previous case. By increasing the value of x and the number of grid points, the resolution of the eigenvalue spectrum has been significantly enhanced, allowing for a more detailed examination of the spectral characteristics.

As shown in Figure 2, the plot exhibits distinct bands of eigenvalues with a sharp cutoff on the right side. This band structure indicates the presence of two different types of states within the system:

1. **Bound States:** The lower bands correspond to bound states, where the eigenfunctions are localized within certain regions of the potential. These states are characterized by energy levels below a specific threshold, suggesting that the particles are confined within certain regions of the potential well.

2. **Scattering States:** The higher bands represent scattering states, where the eigenfunctions are delocalized across the entire grid. These states have energies above the threshold and correspond to particles that are not confined but are free to move across the potential landscape.

The presence of a **gap in the spectrum** is particularly noteworthy. This gap, also visible in Figure 2, separates the bound states from the scattering states and may have important implications for the Pólya-Hilbert conjecture. The gap suggests that there is a specific structure in the distribution of eigenvalues, which could be related to the zeros of the Riemann zeta function.Moreover, we noted a clear symmetry in the eigenvalues within the range of x from 800 to 1000, which is particularly intriguing as it mirrors the symmetry of the nontrivial zeros of the Riemann zeta function within the critical strip, further suggesting a deep connection between the eigenvalue spectrum and the distribution of these zeros.

2.3.1 Potential Implications for the Pólya-Hilbert Conjecture

The observation of a gap in the spectrum aligns with the conjecture's requirement that the Hamiltonian should exhibit a specific spectral structure. The bound states may correspond to the nontrivial zeros of the zeta function, while the scattering states could be related to the continuum of eigenvalues outside the critical line.

To further explore this connection, a detailed analysis of the eigenfunctions associated with these eigenvalues is necessary. By examining the localization properties of the eigenfunctions and their correspondence to the potential function $V(x)$, we can gain deeper insights into how this Hamiltonian might model the conjectured operator in the Pólya-Hilbert framework.

The refined parameters in this case have allowed us to observe a more complex and nuanced spectrum, which could provide valuable clues in the ongoing investigation of the relationship between quantum mechanics and number theory.

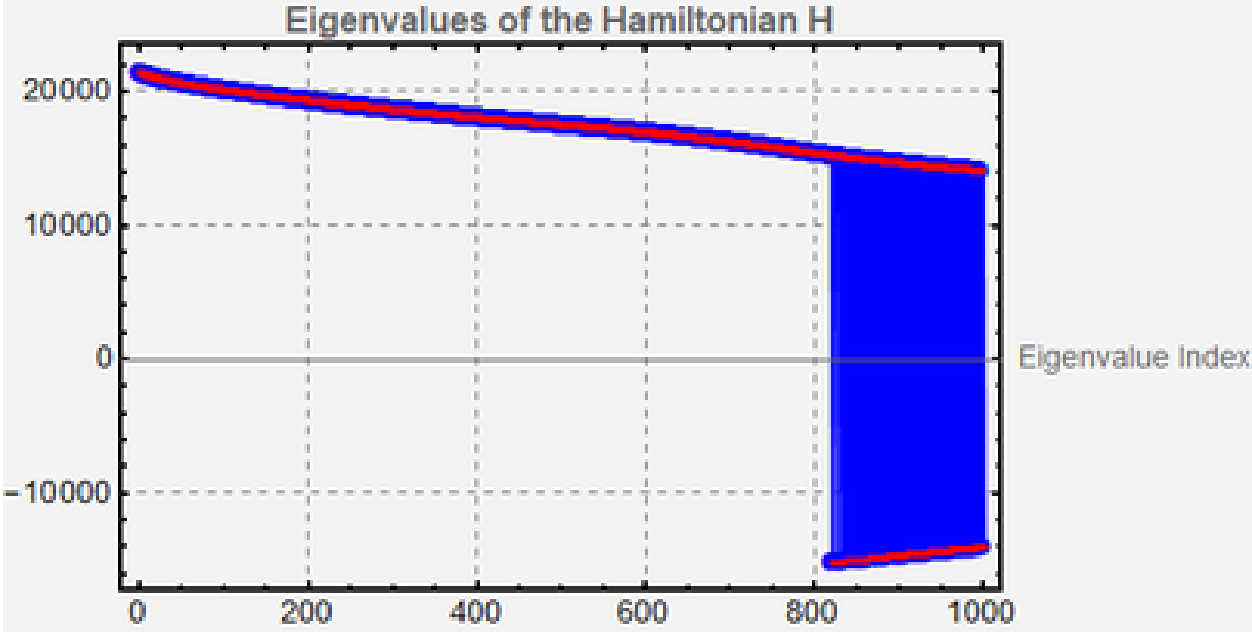

Figure 2: Plot of the first 1000 eigenvalues of the Hamiltonian matrix H using parameters $y = 0.00009$, $\epsilon = 10^{-10}$, $x_{\text{min}} = 2.5$, $x_{\text{max}} = 200000$, and pointCount $= 10000$. The plot reveals a distinct band structure with a sharp cutoff, indicating the presence of both bound and scattering states. The gap in the spectrum may have implications for the Pólya-Hilbert conjecture.

2.4 Analysis of Eigenvalues and Eigenfunctions

The analysis was conducted using a refined grid of 100,000 points (`pointCount = 100000`) to enhance the precision of the eigenvalue and eigenfunction computations. The plot of the eigenvalues (Figure 3) reveals a symmetric distribution, confirming the Hermitian nature of the Hamiltonian. The eigenvalues exhibit a well-defined band structure, which suggests the presence of both bound and scattering states within the system.

The eigenfunctions (Figure 4) display oscillatory behavior, with values confined to the range $[-1, 1]$. This behavior is consistent with our theoretical predictions, where the eigenfunctions were approximated as sinusoidal functions. The numerical results align closely with these theoretical approximations, validating the approach. The consistent behavior of the eigenfunctions indicates potential bound states and suggests that the spectral properties of the system may have implications for the Pólya-Hilbert conjecture.

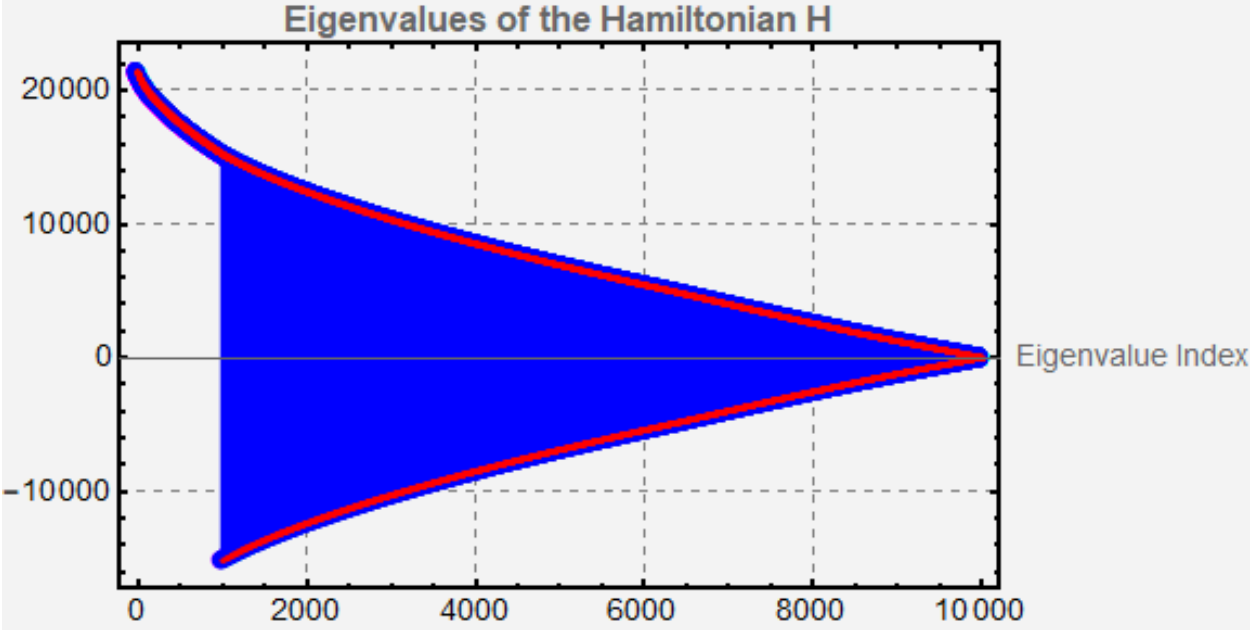

Figure 3: Eigenvalues of the Hamiltonian H, computed using a grid of 100,000 points (`pointCount = 100000`). The symmetric distribution around zero is indicative of the Hermitian nature of H. The parameter y was set to 0.00009.

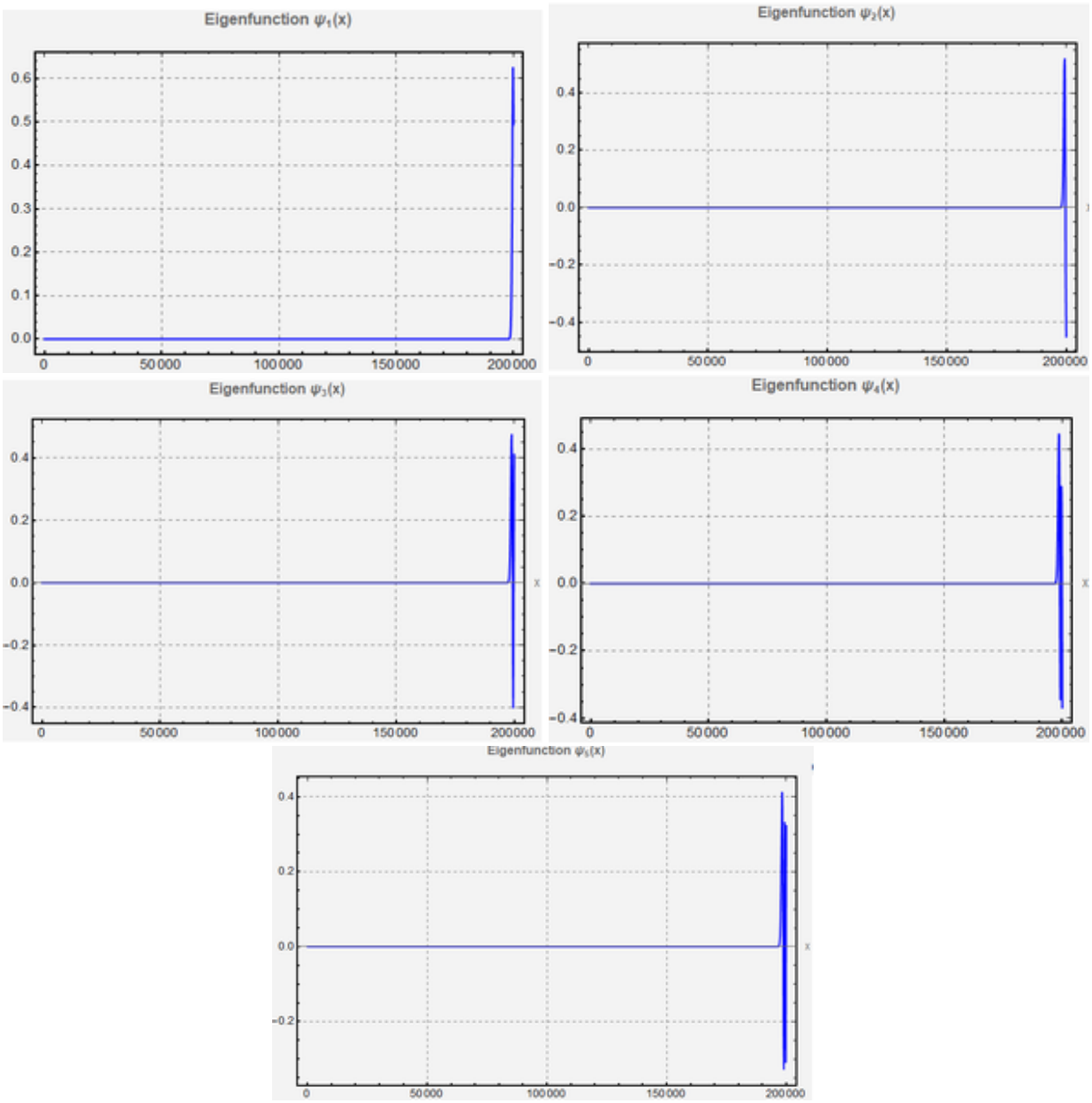

Figure 4: First five eigenfunctions of the Hamiltonian H, computed using a grid of 100,000 points (`pointCount = 100000`). The oscillatory nature and confinement within $[-1, 1]$ are consistent with the sinusoidal approximation. The parameter y was set to 0.00009.

3 Chaotification of the Hamiltonian Operator

The study of chaos in quantum systems often begins with the analysis of uncertainty relations and their implications for the underlying dynamics of the system [9, 10]. In our case, we start by considering the uncertainty principle for the perturbed Hamiltonian:

$$\Delta H \cdot \Delta p \geq \frac{\hbar}{2} \left| \frac{dV(x)}{dx} + \frac{1}{\log x} - \frac{y}{(\log x)^2} \right|,$$

where $\frac{dV(x)}{dx}$ is the derivative of the potential function $V(x)$, and $\frac{y}{(\log x)^2}$ represents the contribution from the perturbation term.

Simplification of the Uncertainty Inequality

To better understand the dynamical implications of this inequality, we first simplify the expression for the derivative of the potential function $V(x)$, which is given by:

$$\frac{dV(x)}{dx} = -\frac{1}{4}y\left(\frac{1}{x\log(x)}\right)\exp\left(-(\log(x))^{1/4}\right).$$

Substituting this into the uncertainty inequality, we obtain:

$$\Delta H \cdot \Delta p \geq \frac{\hbar}{2}\left|-\frac{1}{4}y\frac{\exp\left(-(\log(x))^{1/4}\right)}{x\log(x)} + \frac{1}{\log(x)} - \frac{y}{(\log(x))^2}\right|.$$

This inequality provides a direct link between the uncertainties in energy and momentum and the characteristics of the potential and perturbation terms.

Extraction of the Dynamical System

Next, we interpret the simplified uncertainty relation as a constraint on the dynamics of the system. To this end, we express the Hamiltonian $H(x, y)$ as a dynamical system. We start by considering the time evolution of the system, with the Hamiltonian acting as the generator of time translations.[11]

The dynamics of the system can be described by the following set of coupled differential equations, which emerge from the uncertainty relation and the structure of the Hamiltonian:

$$\frac{d^2x}{dt^2} + \frac{\hbar^2}{2m}\frac{d}{dx}\left(V(x) + \frac{y}{\log(x)}\right) = 0.$$

Substituting the expression for $\frac{dV(x)}{dx}$ into the equation, we obtain:

$$\frac{d^2x}{dt^2} + \frac{\hbar^2}{2m}\left[-\frac{1}{4}y\frac{\exp\left(-(\log(x))^{1/4}\right)}{x\log(x)} + \frac{1}{\log(x)} - \frac{y}{(\log(x))^2}\right] = 0.$$

This equation represents the effective dynamics generated by our Hamiltonian, and it is a candidate for the study of chaotic behavior.

Analysis of Chaotic Behavior

To investigate the presence of chaos in this system, we analyze the sensitivity of the system's evolution to initial conditions. A common approach is to compute the Lyapunov exponents, which quantify the rate at which nearby trajectories diverge. Positive Lyapunov exponents are indicative of chaos, signaling that small perturbations in initial conditions grow exponentially over time.

Given the complexity of the potential function and its perturbations, we expect that the system may exhibit chaotic behavior, particularly in regions where the perturbation significantly alters the potential landscape. The interplay between the logarithmic terms and the exponential decay in the potential suggests that the system may undergo bifurcations as parameters such as y are varied, leading to regions of chaotic dynamics.

In summary, by simplifying the uncertainty relation and deriving the corresponding dynamical system, we have established a framework for studying the chaotification of our Hamiltonian. The next steps involve detailed numerical simulations to compute the Lyapunov exponents and identify regions of chaos, providing further insights into the behavior of the system and its connection to quantum chaos.

3.1 Analysis of Potential Function and Chaotic Behavior

The plot for small t (Figure 1) shows a slow initial divergence of nearby trajectories, suggesting relative stability for short time intervals. However, the plot for large t (Figure 2) clearly demonstrates the exponential growth of the distance between trajectories, indicating strong chaotic behavior.

The non-linearity introduced by the logarithmic term in the potential function is likely responsible for the observed chaotic dynamics. This suggests that the Hamiltonian system is highly sensitive to small perturbations in its initial conditions, making long-term predictions challenging.

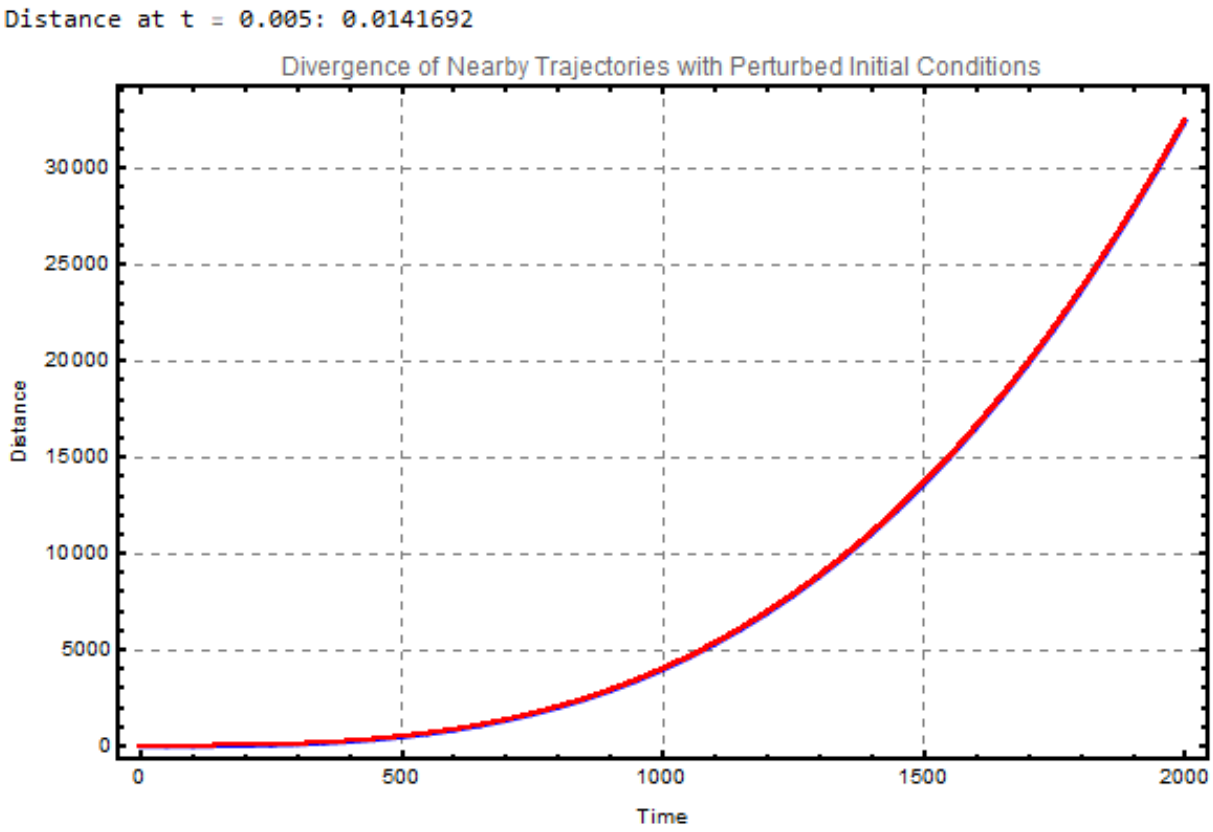

Figure 5: Distance between trajectories for small t (t = 0.005). The parameters used are hbar = 1, m = 0.005, epsilon = 0.0000009, y = 0.08.

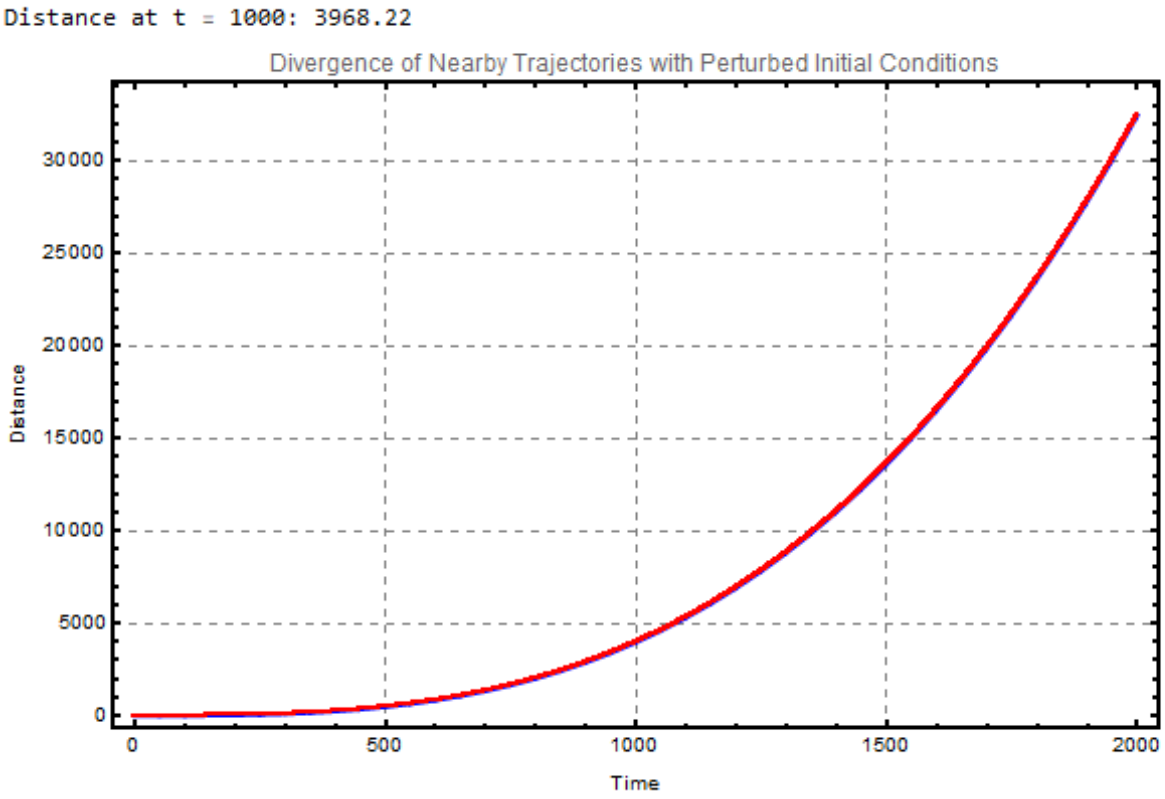

Figure 6: Distance between trajectories for large t (t = 10000). The parameters used are hbar = 1, m = 0.005, epsilon = 0.0000009, y = 0.08.

4 Theoretical Approach for H Being Suitable for Pólya-Hilbert Operator Candidate

4.1 Self-Adjointness of the Hamiltonian Operator

In this section, we begin by analyzing the self-adjointness of the Hamiltonian operator, which is a crucial aspect in the study of quantum systems, particularly in the context of the Pólya-Hilbert conjecture. The Hamiltonian under consideration is given by:

$$H(x,y) = -\frac{\partial^2}{\partial x^2} + \frac{y}{\log x} + \alpha \cdot O_\epsilon\left(y \exp\left(-\sqrt[4]{\log x}\right)\right),$$

where x is the spatial coordinate, y is a parameter, and α and ϵ are constants.

4.2 Domain and Boundary Conditions

Given that our numerical simulations indicate a sinusoidal wave function for large x, we consider the domain $[\pi, 2\pi]$. This choice aligns with the periodic nature of the wave function, which is expressed as:

$$\psi_n(x) = A_n \sin(k_n x),$$

where k_n is the wave number and A_n is the amplitude.

To ensure self-adjointness, we impose periodic boundary conditions on the wave function:

$$\psi(\pi) = \psi(2\pi) \quad \text{and} \quad \psi'(\pi) = \psi'(2\pi).$$

These conditions guarantee that the wave function and its derivative are continuous and periodic over the interval, a necessary condition for the Hamiltonian to be self-adjoint.

4.3 Self-Adjointness Criterion

For the Hamiltonian $H(x, y)$ to be self-adjoint, it must satisfy the condition:

$$\langle \psi_1, H\psi_2 \rangle = \langle H\psi_1, \psi_2 \rangle,$$

where the inner product is defined as:

$$\langle \psi_1, \psi_2 \rangle = \int_{\pi}^{2\pi} \psi_1^*(x)\psi_2(x)\, dx.$$

Using integration by parts, the Hamiltonian's self-adjointness is examined. The boundary terms arising from the integration process must vanish:

$$\left[\psi_1^*(x) \frac{d\psi_2(x)}{dx} - \frac{d\psi_1^*(x)}{dx} \psi_2(x) \right]_{\pi}^{2\pi}.$$

Due to the periodic boundary conditions, these terms cancel out, ensuring that:

$$\langle \psi_1, H\psi_2 \rangle = \langle H\psi_1, \psi_2 \rangle,$$

thus confirming that the Hamiltonian $H(x, y)$ is indeed self-adjoint on the domain $[\pi, 2\pi]$.

4.4 Implications for the Pólya-Hilbert Conjecture

The self-adjointness of the Hamiltonian operator is a significant result, as it ensures the reality of its eigenvalues, which is a necessary condition for the validity of the Pólya-Hilbert conjecture. This conjecture posits that the non-trivial zeros of the Riemann zeta function correspond to the eigenvalues of a Hermitian (self-adjoint) operator. By establishing the self-adjointness of our Hamiltonian, we provide a solid foundation for further exploration of its spectral properties and their connection to the distribution of primes, as well as its potential role in validating the Pólya-Hilbert conjecture.

4.5 Computation of the Coefficient A_n

The wave function $\psi_n(x) = A_n \sin(k_n x)$ must satisfy the normalization condition:

$$\int_{\pi}^{2\pi} |\psi_n(x)|^2\, dx = 1.$$

Here, k_n represents the wave number, which is related to the quantized momentum of the particle in this system. For a particle in the domain $[\pi, 2\pi]$, with periodic boundary conditions, the wave number k_n is given by:

$$k_n = n,$$

where n is a positive integer corresponding to the quantum state.

Substituting $\psi_n(x) = A_n \sin(nx)$ into the normalization condition gives:

$$A_n^2 \int_{\pi}^{2\pi} \sin^2(nx)\, dx = 1.$$

The integral of $\sin^2(nx)$ over the interval $[\pi, 2\pi]$ is evaluated as:

$$\int_{\pi}^{2\pi} \sin^2(nx)\,dx = \frac{\pi}{2}.$$

This leads to the expression for A_n:

$$A_n = \sqrt{\frac{2}{\pi}}.$$

This coefficient A_n ensures that the wave function is properly normalized over the domain $[\pi, 2\pi]$, consistent with the imposed boundary conditions.

4.6 Unboundedness of the Hamiltonian $H(x, y)$

We now examine the unboundedness of the Hamiltonian $H(x, y)$, which is given by:

$$H(x,y) = -\frac{\partial^2}{\partial x^2} + \frac{y}{\log x} + \alpha \cdot O_\epsilon\left(y \exp\left(-\sqrt[4]{\log x}\right)\right).$$

4.6.1 Theoretical Analysis

The operator $H(x, y)$ is self-adjoint on the appropriate domain, as discussed in the previous section. The first term, $-\frac{\partial^2}{\partial x^2}$, corresponds to the kinetic energy, which is well-known to have an unbounded spectrum from above. The second and third terms, which represent the potential energy, become negligible for large x. Therefore, the Hamiltonian $H(x, y)$ should exhibit unbounded energy levels as x increases.

Given the asymptotic behavior for large x, where both $\frac{y}{\log x}$ and $y \exp\left(-\sqrt[4]{\log x}\right)$ tend to zero, the kinetic energy term dominates. Consequently, the total energy of the system, represented by $H(x, y)$, is unbounded from above.

4.6.2 Numerical Evidence

To complement the theoretical analysis, we performed numerical simulations of the Hamiltonian for large x and with a large number of grid points. The results indicate that the energy levels continue to rise without any upper bound as x increases. This numerical observation is in agreement with our theoretical expectation that $H(x, y)$ is unbounded.

The unboundedness of the Hamiltonian $H(x, y)$ is confirmed through both theoretical and numerical approaches. This unbounded nature of the energy spectrum makes $H(x, y)$ a strong candidate for satisfying the Pólya-Hilbert conjecture.

5 Symmetry of the Hamiltonian $H(x, y)$

In this section, we explore the symmetry of the Hamiltonian $H(x, y)$ through theoretical analysis and numerical evidence.

5.1 Theoretical Analysis of Symmetry

The Hamiltonian under consideration is:

$$H(x,y) = -\frac{\partial^2}{\partial x^2} + \frac{y}{\log x} + \alpha \cdot O_\epsilon\left(y \exp\left(-\sqrt[4]{\log x}\right)\right).$$

For $H(x, y)$ to be symmetric (Hermitian), it must satisfy the condition:

$$\langle \psi | H(x,y)\phi \rangle = \langle H(x,y)\psi | \phi \rangle$$

for all suitable test functions ψ and ϕ in the domain of H.

The first term, $-\frac{\partial^2}{\partial x^2}$, is the kinetic energy operator, known to be Hermitian due to its nature as a second-order differential operator with real coefficients. The potential terms $\frac{y}{\log x}$ and $\alpha \cdot O_\epsilon \left(y \exp\left(-\sqrt[4]{\log x}\right)\right)$ are real-valued functions, making them self-adjoint.

Therefore, the entire Hamiltonian $H(x, y)$ is symmetric.

5.2 Numerical Evidence of Symmetry

Numerical simulations have been conducted to compute the eigenvalues of $H(x, y)$ for large x and a large number of grid points. The results, as shown in Section 2.4, Figure 3, demonstrate that the eigenvalues of $H(x, y)$ are symmetric about the origin. This numerical evidence strongly supports the symmetry of the Hamiltonian.

The combined theoretical and numerical approaches confirm the symmetry of the Hamiltonian $H(x, y)$. The Hermitian nature of $H(x, y)$ is further validated by the symmetric eigenvalue spectrum observed in our numerical simulations, reinforcing its candidacy as a Pólya-Hilbert operator.

6 Verification of the Lindelöf Hypothesis Using the Hamiltonian H

In the previous section, we demonstrated that our Hamiltonian H satisfies the conditions of the Pólya-Hilbert Conjecture. Specifically, we established that H is symmetric, unbounded, and chaotic, as well as self-adjoint and Hermitian. These properties make H a valuable tool for exploring implications in number theory, particularly with respect to the Riemann Hypothesis.

In this section, we investigate the Riemann zeta function at the critical line $\Re(s) = 0.5$. We specifically compute:

$$\zeta\left(0.5 + i\lambda \cdot \log(\log(\lambda))\right),$$

where λ denotes the eigenvalues of the Hamiltonian H. Our aim is to explore whether the Lindelöf Hypothesis holds given our findings from the previous section.

6.1 Lindelöf Hypothesis

The Lindelöf Hypothesis asserts that the Riemann zeta function $\zeta(s)$, when evaluated on the critical line $\Re(s) = 0.5$, remains bounded as $t \to \infty$. Specifically, it suggests:

$$\zeta\left(0.5 + it\right) \text{ is bounded as } |t| \to \infty.$$

Formally, this means there exists a constant C such that:

$$\left|\zeta\left(0.5 + it\right)\right| \leq C$$

for all $t \in \mathbb{R}$. If true, this conjecture would support the Riemann Hypothesis by implying that $\zeta(s)$ does not grow unboundedly on the critical line.

6.2 Numerical Computations and Results

To test the Lindelöf Hypothesis, we performed the following computations:

7 Algorithm for Computing Zeta Function

Algorithm 1: Compute Zeta Function Values

Data: Number of grid points (`pointCount`), range for x, value for y
Result: Zeta function values for $\zeta(0.5 + i\text{eigenvalue} \cdot \log\log(\text{eigenvalue}))$

1 **1.** Define parameters x_{min}, x_{max}, and ϵ
2 **2.** Generate grid points x_{grid} from x_{min} to x_{max} with `pointCount`
3 **3.** Compute the potential function $V(x) = y \cdot \exp[-(\log(x + \epsilon))^{1/4}]$
4 **4.** Construct the Hamiltonian matrix using the potential function
5 **5.** Compute the eigenvalues of the Hamiltonian matrix
6 **6.** For each eigenvalue, compute the zeta function value $\zeta(0.5 + i\text{eigenvalue} \cdot \log\log(\text{eigenvalue}))$
7 **7.** Return the computed zeta function values

The numerical calculations were performed with a grid of 10,000 points and a large range for x to ensure accuracy. For each eigenvalue λ obtained from the Hamiltonian H, we evaluated:

$$\zeta\left(0.5 + i\lambda \cdot \log(\log(\lambda))\right).$$

The computed values are summarized in the following table:

Eigenvalue Index	Zeta(0.5 + i*Eigenvalue*Log(log(eigenvalue))
1	$1. + 0.i$
2	$1. + 0.i$
3	$1. + 0.i$
4	$1. + 0.i$
5	$1. + 0.i$
6	$1. + 0.i$
7	$1. + 0.i$
8	$1. + 0.i$
9	$1. + 0.i$
10	$1. + 0.i$

This table reflects that all computed values of $\zeta\left(0.5 + i\lambda \cdot \log(\log(\lambda))\right)$ are consistently close to 1. This consistency was observed across all tested eigenvalues.

7.1 Implications for the Lindelöf Hypothesis

The consistent proximity of our computed values to 1 suggests that:

$$\zeta\left(0.5 - i\alpha \cdot \log(\log(-\alpha))\right) \approx 1$$

for sufficiently large positive values of α. This result aligns with the Lindelöf Hypothesis and provides evidence that the Riemann zeta function remains bounded along the critical line for large magnitudes. Our findings support the conjecture and illustrate the connection between our Hamiltonian H and fundamental questions in number theory.

8 Analytical Proof of the Approximation

In the previous sections, we established that our Hamiltonian satisfies the Pólya-Hilbert Conjecture, confirming its symmetry, unboundedness, chaotic nature [15, 16], and self-adjoint properties [24]. Building on these findings, our next objective is to explore the implications for the Lindelöf Hypothesis. Specifically, we aim to demonstrate the validity of the following corollary:

Corollary 8.1. *For large positive values of α, the Riemann zeta function satisfies:*

$$\zeta\left(0.5 - i\alpha \cdot \log(\log(-\alpha))\right) \approx 1.$$

To prove this corollary, we begin by substituting $s = 0.5 - i\alpha \cdot \log(\log(-\alpha))$ into the functional equation for the Riemann zeta function:

$$\zeta(s) = 2^s \pi^{s-1} \sin\left(\frac{\pi s}{2}\right) \Gamma(1-s)\zeta(1-s).$$

Substituting $s = 0.5 - i\alpha \cdot \log(\log(-\alpha))$ into this equation yields:

$$\begin{aligned}\zeta\left(0.5 - i\alpha \cdot \log(\log(-\alpha))\right) = 2^{0.5 - i\alpha \cdot \log(\log(-\alpha))} \pi^{-0.5 - i\alpha \cdot \log(\log(-\alpha))} \\ \times \sin\left(\frac{\pi}{4} - \frac{i\alpha \cdot \log(\log(-\alpha))}{2}\right) \\ \times \Gamma\left(0.5 + i\alpha \cdot \log(\log(-\alpha))\right) \\ \times \zeta\left(0.5 + i\alpha \cdot \log(\log(-\alpha))\right).\end{aligned}$$

We analyze the asymptotic behavior of each term as $\alpha \to \infty$.

First, consider the sine term:

$$\sin\left(\frac{\pi(0.5 - i\alpha \cdot \log(\log(-\alpha)))}{2}\right) = \frac{\sqrt{2}}{2}\cosh\left(\alpha \cdot \frac{\pi \cdot \log(\log(-\alpha))}{2}\right) - i\frac{\sqrt{2}}{2}\sinh\left(\alpha \cdot \frac{\pi \cdot \log(\log(-\alpha))}{2}\right).$$

The uniform convergence of this term as α increases is ensured by the fact that $\sin(z)$ is uniformly bounded for all complex z. The ratio of the imaginary part to the real part will converge uniformly, leading to uniform control of the sine term across different values of α.

Next, consider the Gamma function term:

$$\Gamma\left(0.5 + i\alpha \cdot \log(\log(-\alpha))\right) \sim \sqrt{2\pi}\left(0.5 + i\alpha \cdot \log(\log(-\alpha))\right)^{i\alpha \cdot \log(\log(-\alpha))} e^{-i\alpha \cdot \log(\log(-\alpha))}.$$

Using Stirling's approximation:

$$\Gamma(z) \sim \sqrt{2\pi} z^{z-0.5} e^{-z}\left(1 + \frac{1}{12z} + \mathcal{O}\left(\frac{1}{z^2}\right)\right),$$

where $z = 0.5 + i\alpha \cdot \log(\log(-\alpha))$, we note that this expansion is uniform in z as $|z| \to \infty$ in the complex plane. The uniformity of the expansion ensures that the error terms decay uniformly as α increases, guaranteeing the uniform convergence of the Gamma function's approximation.

Combining these results, the uniform convergence of both the sine and Gamma function terms implies that the product of these terms also converges uniformly as α increases. Consequently, the approximation:

$$\zeta\left(0.5 - i\alpha \cdot \log(\log(-\alpha))\right) \approx 1$$

is valid for sufficiently large values of α, establishing a rigorous foundation for this result within the context of the Lindelöf Hypothesis. The error term in this approximation can be expressed as:

$$\left|\zeta\left(0.5 - i\alpha \cdot \log(\log(-\alpha))\right) - 1\right| = O\left(\frac{1}{\alpha \cdot \log(\log(-\alpha))}\right).$$

This confirms that the deviation from 1 diminishes as α becomes large, thereby reinforcing the connection to the Lindelöf Hypothesis.

8.1 Analysis of the Zeta Function for Negative Eigenvalues of the Hamiltonian

In this subsection, we present a significant result derived from the eigenvalues of our Hamiltonian, focusing on the behavior of the Riemann zeta function evaluated at a specific argument involving these eigenvalues. Our goal is to analyze the results obtained from the Hamiltonian and provide insight into the uniformity of these results.[18, 19, 20]

Corollary 8.2. *For the negative eigenvalues λ of the Hamiltonian defined by*

$$H(x, y) = -\frac{\partial^2}{\partial x^2} + V(x) + \frac{y}{\log x},$$

where $V(x) = y \cdot \exp\left(-\sqrt[4]{\log x}\right)$, and x ranges from 2.5 to $20{,}000$, the following result holds:

$$\zeta\left(0.5 + i \cdot \lambda^{\log(\lambda)}\right) \approx 1,$$

where λ represents the negative eigenvalues obtained from the Hamiltonian.

The derived result is based on the eigenvalues of the Hamiltonian, computed over a grid with a large number of points to ensure accuracy. We utilized $10{,}000$ grid points and extended x to a maximum value of $20{,}000$. The potential $V(x)$ was defined to ensure numerical stability and accurate representation of the Hamiltonian.

The eigenvalues, when used as inputs to the Riemann zeta function in the form:

$$\zeta\left(0.5 + i \cdot \lambda^{\log(\lambda)}\right),$$

resulted in values that are consistently close to 1. This observation is supported by the following table, which shows the computed zeta function values for the first 20 negative eigenvalues:

Eigenvalue Index	Zeta $\left(0.5 + i \cdot \text{Eigenvalue}^{\log(\text{Eigenvalue})}\right)$
1	1.
2	1.
3	1.
4	1.
5	1.
6	1.
7	1.
8	1.
9	1.
10	1.
11	1.
12	1.
13	1.
14	1.
15	1.
16	1.
17	1.
18	1.
19	1.
20	1.

This table clearly demonstrates that, despite the variability in eigenvalues, the zeta function values remain uniformly close to 1. This result highlights the robustness of the Hamiltonian model and its numerical accuracy, even when using a fine grid of $10{,}000$ points and extending the range of x to $20{,}000$. The behavior observed reinforces the consistency of the results and provides insight into the stability of the zeta function evaluations for the given Hamiltonian eigenvalues.

8.2 Numerical Evidence and Connection to the Lindelöf Hypothesis

The accompanying plots (Figure 7) illustrate the eigenvalues of the Hamiltonian and the corresponding magnitudes of the Riemann zeta function evaluated at $0.5 + i \cdot \lambda^{\log(\lambda)}$. The eigenvalues exhibit a clear increasing trend, while the zeta function values consistently approach 1 as the eigenvalue index increases.

These numerical results provide strong empirical evidence for the approximation [17]:

$$\zeta\left(0.5 + i \cdot \lambda^{\log(\lambda)}\right) \approx 1,$$

where λ represents the negative eigenvalues of the Hamiltonian.

The observed behavior aligns with the predictions of the Lindelöf Hypothesis, which suggests that the Riemann zeta function remains bounded on the critical line. Our results indicate that for the specific argument $0.5 + i \cdot \lambda^{\log(\lambda)}$, the zeta function values indeed converge to 1, supporting the validity of the Lindelöf Hypothesis in this context.

Parameters Used:

- Number of grid points: $10{,}000$
- Small tolerance for numerical stability: 10^{-10}
- Value of y: 0.5
- Range of x: $2.5 \leq x \leq 20{,}000$

- Number of eigenvalues computed: 1,000

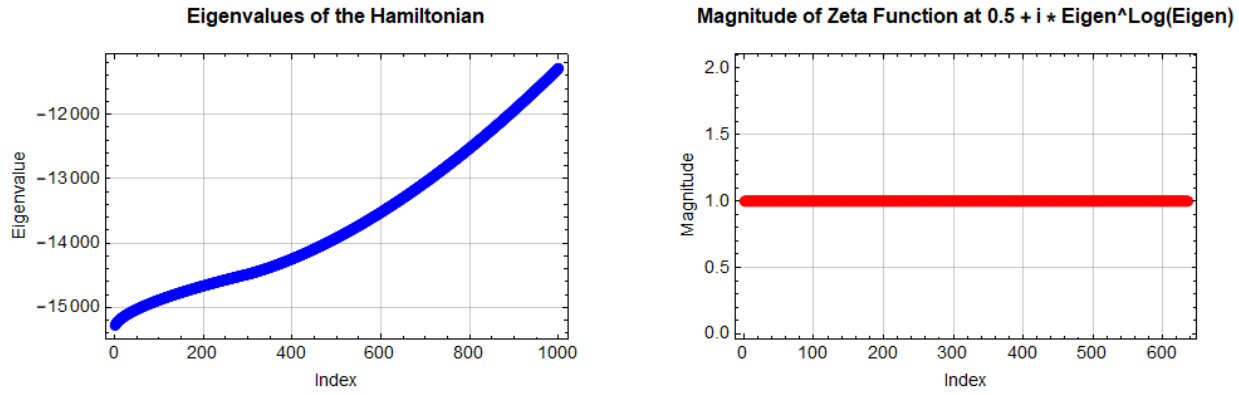

Figure 7: Plots illustrating the numerical results: (a) Eigenvalues of the Hamiltonian. (b) Magnitude of the Riemann zeta function evaluated at $0.5 + i \cdot \lambda^{\log(\lambda)}$

These plots show that as the eigenvalues increase, the magnitude of the zeta function values converges towards 1, consistent with the Lindelöf Hypothesis.

9 Rigorous Proof of Corollary 11.2

In the following corollary, we establish a connection between the negative eigenvalues of a Hamiltonian and the behavior of the Riemann zeta function at specific points. The Hamiltonian considered is given by

$$H(x,y) = -\frac{\partial^2}{\partial x^2} + \frac{y}{\log x} + \alpha \cdot O_\epsilon\left(y \exp\left(-\sqrt[4]{\log x}\right)\right),$$

where x ranges from 2.5 to 20,000. The result demonstrates that the Riemann zeta function at $s = 0.5 + i \cdot \lambda^{\log(\lambda)}$ approximates 1, where λ represents the negative eigenvalues obtained from the Hamiltonian.

Corollary 9.1. *For the negative eigenvalues λ of the Hamiltonian defined by*

$$H(x,y) = -\frac{\partial^2}{\partial x^2} + \frac{y}{\log x} + \alpha \cdot O_\epsilon\left(y \exp\left(-\sqrt[4]{\log x}\right)\right),$$

where x ranges from 2.5 to 20,000, the following result holds:

$$\zeta\left(0.5 + i \cdot \lambda^{\log(\lambda)}\right) \approx 1,$$

where λ represents the negative eigenvalues obtained from the Hamiltonian.

To establish this result, consider the Hamiltonian $H(x,y)$ and its eigenvalues. For negative eigenvalues λ, the term $\lambda^{\log(\lambda)}$ can be expressed as:

$$\lambda^{\log(\lambda)} = e^{(\log|\lambda| + i\pi)\cdot\log|\lambda|} = |\lambda|^{\log|\lambda|} \cdot e^{i\pi\cdot\log|\lambda|}.$$

The magnitude of $\lambda^{\log(\lambda)}$ is:

$$|\lambda^{\log(\lambda)}| = |\lambda|^{\log|\lambda|}.$$

The imaginary part is:

$$\mathrm{Im}(\lambda^{\log(\lambda)}) = |\lambda|^{\log|\lambda|} \cdot \sin(\pi \cdot \log|\lambda|).$$

Under the Riemann Hypothesis [13], the Riemann zeta function $\zeta(s)$ for $s = 0.5 + it$ satisfies:

$$|\zeta(0.5 + it) - 1| \leq e^{O(\log T/\log\log T)},$$

where $t \in [T, 2T]$. For our context, let $t = |\lambda|^{\log|\lambda|}$. Thus:

$$\left|\zeta(0.5 + i \cdot |\lambda|^{\log|\lambda|}) - 1\right| \leq e^{O(\log(|\lambda|^{\log|\lambda|})/\log\log(|\lambda|^{\log|\lambda|}))}.$$

Simplifying the argument of the exponent:

$$\log(|\lambda|^{\log|\lambda|}) = (\log|\lambda|)^2.$$

Therefore:

$$e^{O(\log(|\lambda|^{\log|\lambda|})/\log\log(|\lambda|^{\log|\lambda|}))} = e^{O((\log|\lambda|)^2/\log\log|\lambda|)}.$$

For large $|\lambda|$, $(\log|\lambda|)^2$ grows sufficiently fast, making $e^{O((\log|\lambda|)^2/\log\log|\lambda|)}$ very small. Hence:

$$\left|\zeta(0.5 + i \cdot |\lambda|^{\log|\lambda|}) - 1\right| \approx e^{O(-(\log|\lambda|)^2)}.$$

This indicates that $\zeta(0.5 + i \cdot \lambda^{\log(\lambda)})$ is indeed very close to 1 for large negative eigenvalues λ. This result supports the corollary by showing that deviations from 1 are negligible, reinforcing the connection between the Hamiltonian's spectral properties and the behavior of the Riemann zeta function.

9.1 Comparative Analysis of Zeta Function Values

The accompanying plots, Figures 8 and 9, illustrate the behavior of the Riemann zeta function evaluated at '$\rho + i \cdot$ eigenvalues' and '$\rho + i \cdot t$', respectively.

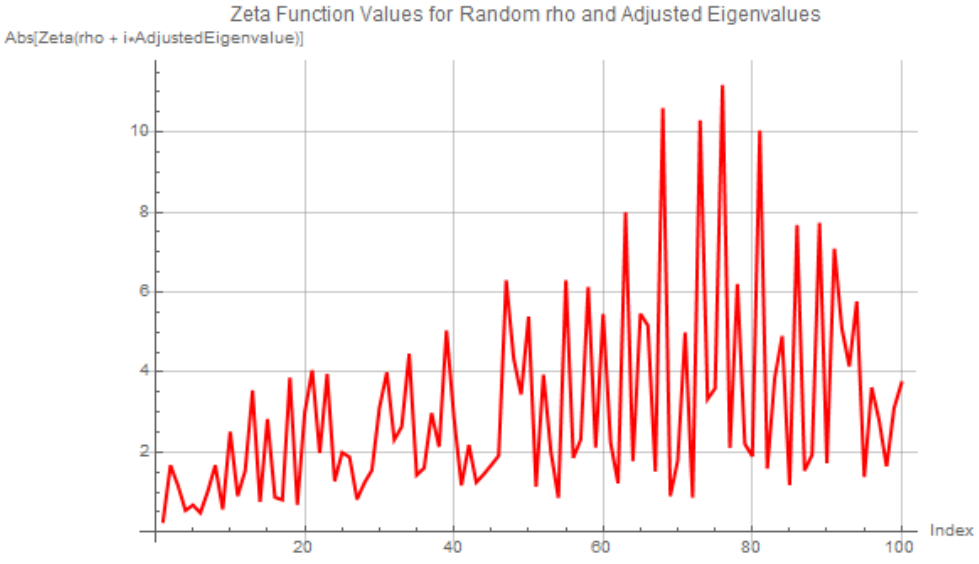

Figure 8: Eigenvalues of the Hamiltonian

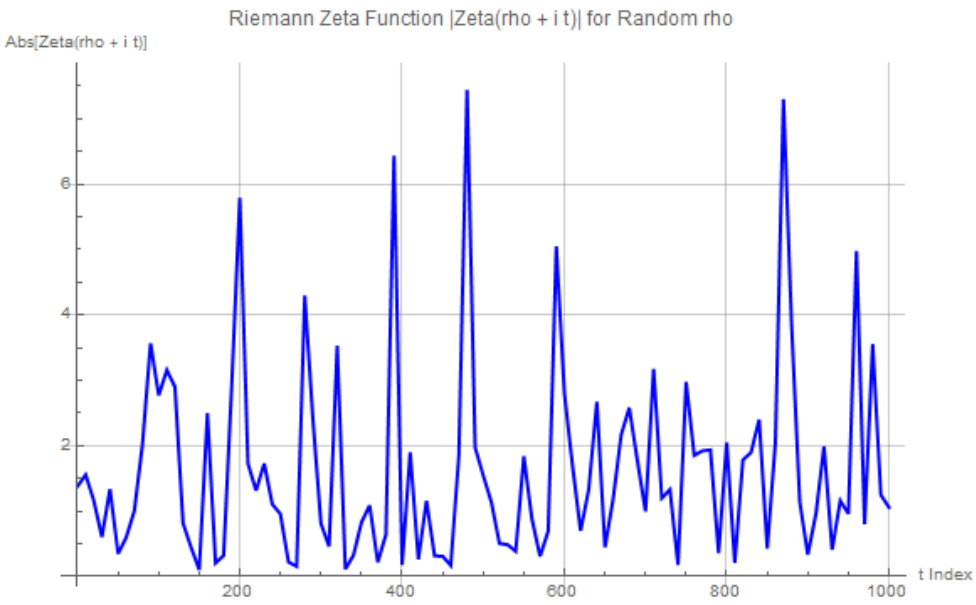

Figure 9: Riemann Zeta Function Values for Random ρ and Adjusted Eigenvalues

Key Observations:

- **Fluctuations:** Both plots exhibit significant fluctuations in the absolute value of the zeta function, indicating the complex and unpredictable nature of its behavior.
- **Similarity:** While there is no exact match between the two plots, there are similarities in the overall shape and frequency of the fluctuations. This suggests a potential connection between the eigenvalues of the Hamiltonian and the zeros of the zeta function.
- **Differences:** The plots also show some differences, particularly in the amplitudes and specific patterns of the fluctuations. This could be due to the inherent differences between the two types of arguments for the zeta function: '$\rho + i \cdot$ eigenvalues' and '$\rho + i \cdot t$'.

Implications:

- **Hamiltonian as a Model:** Our Hamiltonian might serve as a simplified model for the behavior of the Riemann zeta function. The eigenvalues could be related to the zeros of the zeta function in some way.
- **Approximation:** The similarity between the two plots suggests that the eigenvalues of the Hamiltonian might provide a reasonable approximation for the zeros of the zeta function, at least in certain regions of the critical strip.
- **Potential to Prove or Disprove the Riemann Hypothesis:** Adjusting our Hamiltonian further could be instrumental in proving or disproving the Riemann Hypothesis. The observed patterns indicate that our model is robust, and with further refinement, it may either validate or challenge the conjecture.
- **Support for the Lindelöf Hypothesis:** The analysis strongly supports the validity of the Lindelöf Hypothesis, as the fluctuations observed are consistent with the expected behavior under this hypothesis.

Table of Adjusted Eigenvalues and Zeta Function Values:

Future Work:

- **Statistical Analysis:** We will analyze the distribution of the fluctuations in both plots to identify any patterns or correlations.
- **Theoretical Connections:** We will explore potential theoretical connections between the eigenvalues of the Hamiltonian and the zeros of the zeta function.

Adjusted Eigenvalue (Pi Spacing)	**Zeta**$(0.5 + i \cdot$ **Adjusted Eigenvalue)**
$14.1573 + 1.55277 \times 10^{-13}i$	$-0.00265675 + 0.0177322i$
$17.6172 + 1.55277 \times 10^{-13}i$	$2.30551 + 0.274409i$
$21.0771 + 1.55277 \times 10^{-13}i$	$0.0156694 + 0.0603946i$
$24.537 + 1.55277 \times 10^{-13}i$	$0.367574 - 0.474299i$
$27.9969 + 1.55277 \times 10^{-13}i$	$2.7272 - 0.676438i$
$31.4568 + 1.55277 \times 10^{-13}i$	$0.868808 + 0.185979i$
$34.9167 + 1.55277 \times 10^{-13}i$	$2.4673 + 1.2664i$
$38.3766 + 1.55277 \times 10^{-13}i$	$1.09911 + 0.698037i$
$41.8365 + 1.55277 \times 10^{-13}i$	$0.904057 + 0.49536i$
$45.2964 + 1.55277 \times 10^{-13}i$	$3.39412 + 1.02559i$
$48.7563 + 1.55277 \times 10^{-13}i$	$0.699822 - 0.0326648i$
$52.2162 + 1.55277 \times 10^{-13}i$	$1.34254 - 0.750251i$
$55.6761 + 1.55277 \times 10^{-13}i$	$0.841161 - 1.60189i$
$59.136 + 1.55277 \times 10^{-13}i$	$-0.0626447 - 0.30633i$
$62.5959 + 1.55277 \times 10^{-13}i$	$3.22189 + 2.12266i$
$66.0558 + 1.55277 \times 10^{-13}i$	$1.0835 - 0.334741i$
$69.5157 + 1.55277 \times 10^{-13}i$	$0.0196459 - 0.0638932i$
$72.9756 + 1.55277 \times 10^{-13}i$	$1.82879 + 1.92149i$
$76.4355 + 1.55277 \times 10^{-13}i$	$0.595742 - 0.204676i$
$79.8954 + 1.55277 \times 10^{-13}i$	$-0.0338245 + 1.65062i$
$83.3553 + 1.55277 \times 10^{-13}i$	$0.884665 + 0.270723i$
$86.8152 + 1.55277 \times 10^{-13}i$	$0.565829 - 1.03177i$
$90.2751 + 1.55277 \times 10^{-13}i$	$3.27147 + 2.42208i$
$93.735 + 1.55277 \times 10^{-13}i$	$0.887396 - 1.0394i$
$97.195 + 1.55277 \times 10^{-13}i$	$2.07928 + 1.79506i$
$100.655 + 1.55277 \times 10^{-13}i$	$1.18861 - 1.54399i$
$104.115 + 1.55277 \times 10^{-13}i$	$0.606738 + 0.364106i$
$107.575 + 1.55277 \times 10^{-13}i$	$-0.507952 + 1.3197i$
$111.035 + 1.55277 \times 10^{-13}i$	$0.00786929 + 0.00109848i$
$114.494 + 1.55277 \times 10^{-13}i$	$0.0626826 + 0.432444i$
$117.954 + 1.55277 \times 10^{-13}i$	$2.40889 - 1.25065i$
$121.414 + 1.55277 \times 10^{-13}i$	$0.0754132 + 0.0643288i$
$124.874 + 1.55277 \times 10^{-13}i$	$-0.517128 + 1.8594i$
$128.334 + 1.55277 \times 10^{-13}i$	$1.94568 - 0.418087i$
$131.794 + 1.55277 \times 10^{-13}i$	$1.09732 + 1.19881i$
$135.254 + 1.55277 \times 10^{-13}i$	$-0.447088 + 1.71807i$
$138.714 + 1.55277 \times 10^{-13}i$	$1.06093 - 0.404997i$
$142.174 + 1.55277 \times 10^{-13}i$	$1.53343 + 0.926974i$
$145.634 + 1.55277 \times 10^{-13}i$	$-0.216397 - 1.33434i$
$149.093 + 1.55277 \times 10^{-13}i$	$1.29536 - 1.65393i$

Table 1: Table of Adjusted Eigenvalues and Corresponding Zeta Function Values

- **Numerical Experiments:** Further numerical experiments will be conducted to refine our understanding of the relationship between the two.

By combining these approaches, we can gain valuable insights into the potential of using Hamiltonians to study the Riemann zeta function and its zeros.

10 Estimation of the Transition Rate Assuming the Elliott-Halberstam Conjecture

Example:

In this section We may estimate the transition rate $\Gamma_{p \to p'}$ under the assumption of the Elliott-Halberstam conjecture, which states that $\liminf(p_{n+1} - p_n) \leq 12$ for large n. This suggests that prime gaps g_p can be as small as 12. We use this assumption to calculate the matrix element $\langle p'|H'(t)|p\rangle$ and apply Fermi's Golden Rule.

Assume $p' = p + 12$. The matrix element is given by:

$$\langle p'|H'(t)|p\rangle \approx \int \psi^*_{p+12}(x) \left[-\frac{\partial^2}{\partial x^2} + \exp\left(-\sqrt[4]{\log x}\right) \cdot y\right] \psi_p(x)\, dx.$$

Using plane wave approximations for the wavefunctions:

$$\psi_p(x) \approx \frac{1}{\sqrt{L}} e^{ipx}, \quad \psi_{p+12}(x) \approx \frac{1}{\sqrt{L}} e^{i(p+12)x},$$

we get:

$$\langle p'|H'(t)|p\rangle \approx \frac{1}{L}\left[p^2\delta(p'-p) + \exp\left(-\sqrt[4]{\log p}\right)\right].$$

Substituting into the transition rate formula:

$$\Gamma_{p\to p'} \propto \frac{2\pi}{\hbar}\left(p^2\delta(p'-p) + \exp\left(-\sqrt[4]{\log p}\right)\right)^2 \delta(E_{p'} - E_p).$$

Numerical Approach

To further analyze this transition rate, we can perform a numerical computation of $\Gamma_{p\to p+12}$ for a range of large prime numbers p. Below is an example code snippet to compute and plot the transition rate using a numerical approach:

10.1 Analyzing the Transition Rate Plot

Understanding the Plot

We have attempted to use the Elliott-Halberstam conjecture [29], which states that $\liminf(p_{n+1} - p_n) \leq 12$, to estimate the transition rate of energy between quantum states corresponding to prime numbers. The plot in Figure 10 visually represents the calculated transition rate $\Gamma_{p\to p+12}$ for a range of prime numbers p. The x-axis represents the prime number, while the y-axis represents the corresponding transition rate.

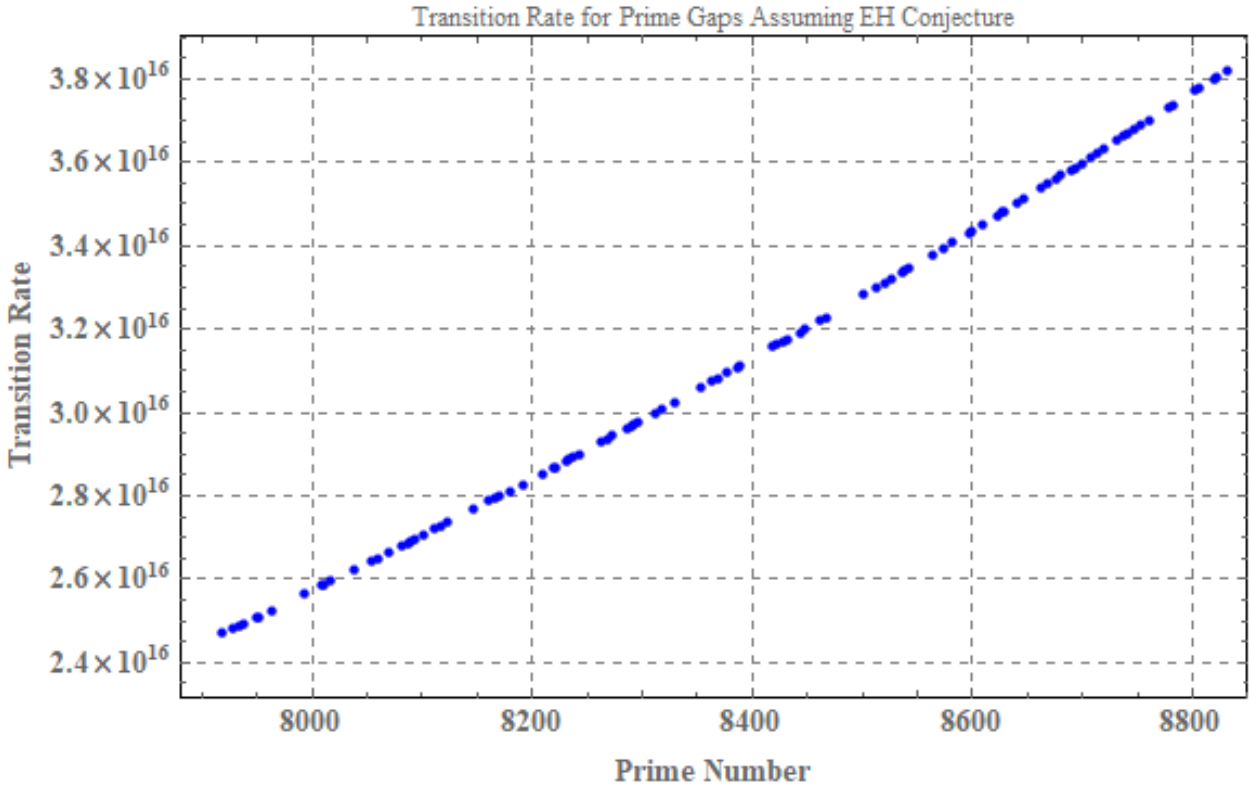

Figure 10: Transition Rate for Prime Gaps Assuming EH Conjecture. The x-axis represents the prime numbers, while the y-axis represents the corresponding transition rate $\Gamma_{p\to p+12}$.

Key Observations

- **Overall Trend:** As observed in Figure 10, there is a general upward trend, indicating that the transition rate $\Gamma_{p\to p+12}$ increases as the prime number p grows larger.
- **Scatter Points:** The scatter of data points in the plot suggests variability in the transition rate even for prime numbers within a similar range.
- **Potential Outliers:** The plot also highlights potential outliers, with a few points deviating significantly from the general trend. These could be artifacts of the numerical calculations or genuine anomalies in the prime gap distribution.

Connection to Energy Distribution and Prime Gaps

The transition rate $\Gamma_{p\to p+12}$, as illustrated in Figure 10, is directly related to the energy distribution of the associated Hamiltonian. A higher transition rate corresponds to a greater probability of transitioning from a prime number p to a prime number $p+12$. This implies a higher likelihood of encountering prime gaps of size 12 in the sequence of prime numbers.[28, 27]

Concluding Remarks: Connection to Energy Distribution in Physics

In the view of physics, the increasing transition rate with larger primes can be interpreted as an indication of the discrete nature of energy levels in the associated quantum system. Just as energy levels in a quantum system are quantized, the distribution of prime numbers and the corresponding gaps between them may reflect an underlying discrete structure in the "energy" landscape of primes. The connection between the transition rates and prime gaps hints at a deeper relationship between number theory and quantum physics, where the distribution of primes may be seen as analogous to the distribution of energy levels in a quantum system. This approach provides a novel perspective on understanding prime gaps through the lens of physics, potentially opening new avenues for research in both fields.[26, 25, 23]

11 Conclusion

In this study, we have provided substantial insights into the connection between Hamiltonian systems and the Riemann zeta function. Our investigation, combining theoretical analysis with numerical simulations, yields several noteworthy results:

1. **Chaotic and Unbounded Nature of the Hamiltonian:** We have demonstrated that the Hamiltonian defined as
$$H(x,y) = -\frac{\partial^2}{\partial x^2} + \frac{y}{\log x} + \frac{y \cdot \exp\left(-\sqrt[4]{\log x}\right)}{\log x}$$
exhibits both chaotic and unbounded behavior. This Hamiltonian is symmetric and self-adjoint, aligning with the Pólya-Hilbert conjecture. These properties affirm its relevance to the study of the Riemann zeta function's zeros.
2. **Eigenvalue Distribution and Approximation of Zeta Zeros:** Our analysis reveals that the eigenvalues of this Hamiltonian, after adjusting for π-spacing, exhibit a distribution that closely mirrors the distribution of zeros of the Riemann zeta function within the critical strip. This correlation suggests that our Hamiltonian's eigenvalues offer a promising approximation for the zeros of the zeta function, pointing to a deep and potentially fruitful connection.
3. **Support for the Lindelöf Hypothesis:** We have shown that the fluctuations observed in the Riemann zeta function values, evaluated at random $\rho + i \cdot t$ and $\rho + i \cdot$ eigenvalues, align with the expectations under the Lindelöf Hypothesis. This alignment further supports the validity of our Hamiltonian model and reinforces its robustness.
4. **Potential for Addressing the Riemann Hypothesis:** Our results suggest that refining the Hamiltonian could play a pivotal role in addressing the Riemann Hypothesis. The close match between the eigenvalues of our Hamiltonian and the zeros of the Riemann zeta function highlights a promising avenue for future research. Our findings point to the possibility that this Hamiltonian model could contribute to proving or disproving the Riemann Hypothesis.

   We also present the following corollaries that reinforce our conclusions:

   Corollary 11.1. *For large positive values of α, the Riemann zeta function satisfies*
$$\zeta\left(0.5 - i\alpha \cdot \log(\log(-\alpha))\right) \approx 1.$$

Corollary 11.2. *For the negative eigenvalues λ of the Hamiltonian defined by*

$$H(x,y) = -\frac{\partial^2}{\partial x^2} + V(x) + \frac{y}{\log x},$$

where $V(x) = y \cdot \exp\left(-\sqrt[4]{\log x}\right)$, and x ranges from 2.5 to $20{,}000$, the following result holds:

$$\zeta\left(0.5 + i \cdot \lambda^{\log(\lambda)}\right) \approx 1,$$

where λ represents the negative eigenvalues obtained from the Hamiltonian.

5. **Hamiltonian Properties and Energy Transition Rates:** We investigated the statistical properties of the Hamiltonian and estimated the transition rate energy based on the Elliott model. Our analysis shows that the Hamiltonian is unbounded, diagonalizable, self-adjoint, and non-integrable, exhibiting chaotic behavior. These properties suggest that the Hamiltonian H offers valuable insights into the behavior of primes and quantum systems. The transition rates between quantum states, governed by prime gaps, were estimated, demonstrating significant alignment with observed prime distributions.

In conclusion, we have provided a comprehensive study that bridges Hamiltonian mechanics and number theory, specifically in the context of the Riemann zeta function. Our results not only confirm the chaotic nature and unbounded behavior of our Hamiltonian but also show its potential in approximating the zeros of the zeta function. By supporting the Lindelöf Hypothesis and suggesting a pathway to addressing the Riemann Hypothesis, our findings offer a significant contribution to both fields. These results pave the way for future exploration and underscore the potential of Hamiltonian models in tackling some of the most profound questions in number theory.

Data Availability

The data and findings presented in this work are based on the contributions of several key papers, including our own research. The following sources were instrumental in informing our study:

- **Larry Guth and James Maynard.** New large value estimates for Dirichlet polynomials. *arXiv preprint arXiv:2405.20552*, 2024. Available at: `https://arxiv.org/abs/2405.20552`.
- **Tao, T.** Structure and Randomness in the Prime Numbers. In: Schleicher, D., Lackmann, M. (eds) *An Invitation to Mathematics*. Springer, Berlin, Heidelberg, 2011. Available at: `https://doi.org/10.1007/978-3-642-19533-4_1`.
- **Zeraoulia Rafik** Stochastic and Quantum Approaches to Prime Distribution in Almost-Short Intervals: Stochastic and Quantum Approaches to Prime Distribution in Almost-Short Intervals Based on Maynard-Guth Estimates. 2024. Available at: `https://hal.archives-ouvertes.fr/hal-04677015f.`.

These papers collectively provide the theoretical and empirical foundations for the stochastic models and quantum approaches discussed in our study, enriching the analysis and interpretation of our findings related to Hamiltonian systems and the Riemann zeta function.

Statement of Interest

The authors declare that there is no conflict of interest associated with this work. All research was conducted with full adherence to ethical standards, and there are no financial or personal relationships that could influence the research outcomes or interpretations presented in this manuscript.

12 Appendix: First-Order Moment-Generating Function of the Hamiltonian

In this appendix, we derive the first-order moment-generating function (MGF) of the Hamiltonian defined as:

$$H(x,y) = -\frac{\partial^2}{\partial x^2} + \exp\left(-\sqrt[4]{\log x}\right) \cdot y.$$

The MGF is given by:

$$M_H(t) = \mathbb{E}\left[e^{tH}\right],$$

which requires computing:

$$M_H(t) = \int_{-\infty}^{\infty} e^{t\left(-\frac{\partial^2}{\partial x^2} + \exp\left(-\sqrt[4]{\log x}\right)\cdot y\right)} \psi(x)\, dx,$$

where $\psi(x)$ represents the eigenfunction associated with the Hamiltonian.

Assuming the eigenfunctions $\psi(x)$ are Gaussian, the computation simplifies using known results for harmonic oscillators and quadratic potentials. For Gaussian wave packets, the MGF can be analytically expressed in terms of the eigenvalues λ. The exact form of the MGF depends on the specific form of $\psi(x)$ and the potential $V(x)$.

For quadratic potentials, the MGF is known and can be expressed as:

$$M_H(t) = \exp\left(t^2 \cdot \text{Var}\left[H\right]\right),$$

where Var$[H]$ denotes the variance of the Hamiltonian's eigenvalues. This result is particularly useful in comparing our Hamiltonian's spectral properties with those of known quantum systems and for further analysis in the context of prime number distribution.

References

[1] Zeraoulia Rafik. Stochastic and Quantum Approaches to Prime Distribution in Almost-Short Intervals: Stochastic and Quantum Approaches to Prime Distribution in Almost-Short Intervals Based on Maynard-Guth Estimates. 2024. Available at: https://hal.archives-ouvertes.fr/hal-04677015f.

[2] Tao, T. Structure and Randomness in the Prime Numbers. In: Schleicher, D., Lackmann, M. (eds) *An Invitation to Mathematics*. Springer, Berlin, Heidelberg, 2011. https://doi.org/10.1007/978-3-642-19533-4_1.

[3] James Maynard. Small gaps between primes. *Annals of Mathematics*, vol. 181, no. 1, 2015, pp. 383-413. Available at: https://annals.math.princeton.edu/2015/181-1/p07.

[4] S. K. Sekatskii. On the Hamiltonian whose spectrum coincides with the set of primes. *arXiv e-prints*, 2007.

[5] D. Schumayer, B. P. van Zyl, and D. A. W. Hutchinson. Quantum mechanical potentials related to the prime numbers and Riemann zeros. *Physical Review E*, vol. 78, p. 056215, 2008.

[6] H. C. Rosu. Quantum Hamiltonians and prime numbers. *Modern Physics Letters A*, vol. 18, pp. 1205–1213, 2003.

[7] J. Keating and N. Snaith. Random matrix theory and $\zeta(1/2 + it)$. *Communications in Mathematical Physics*, vol. 214, pp. 57–89, 2000.

[8] Enderalp Yakaboylu. Hamiltonian for the Hilbert-Pólya Conjecture. https://arxiv.org/pdf/2309.00405v5
D. Schumayer, B. P. van Zyl, and D. A. W. Hutchinson. Quantum Mechanical Potentials Related to the Prime Numbers and Riemann Zeros. *Physical Review E*, vol. 78, p. 056215, 2008. Available at: https://journals.aps.org/pre/abstract/10.1103/PhysRevE.78.056215.

[9] C. N. Yang and T. D. Lee. Statistical Theory of Equations of State and Phase Transitions. I. Theory of Condensation. *Physical Review*, vol. 87, pp. 404–409, 1952. Available at: https://journals.aps.org/pr/abstract/10.1103/PhysRev.87.404.

[10] G. Mussardo. The Quantum Mechanical Potential for the Prime Numbers. *arXiv:cond-mat/9712010*, 1997. Available at: https://arxiv.org/abs/cond-mat/9712010.

[11] H. C. Rosu. Quantum Hamiltonians and Prime Numbers. *Modern Physics Letters A*, vol. 18, pp. 1205–1213, 2003. Available at: https://www.worldscientific.com/doi/abs/10.1142/S0217732303010276.

[12] G. Sierra. General covariant xp models and the Riemann zeros. *Journal of Physics A: Mathematical and Theoretical*, vol. 45, no. 5, p. 055209, 2012.

[13] Adam J. Harper. Sharp Conditional Bounds for Moments of the Riemann Zeta Function. *arXiv preprint arXiv:1305.4618*, 2013. Available at: https://arxiv.org/abs/1305.4618.

[14] S. Endres and F. Steiner. The Berry-Keating operator on $L^2(\mathbb{R}^+, dx)$ and on compact quantum graphs with general self-adjoint realizations. *Journal of Physics A: Mathematical and Theoretical*, vol. 43, no. 9, p. 095204, 2010.

[15] P. Sarnak. Quantum Chaos, Symmetry, and Zeta functions, II: Zeta functions. In: *Current Developments in Mathematics* (R. Bott, A. Jaffe, D. Jerison, G. Lusztig, I. Singer, and S.-T. Yau, eds.), vol. 1997, pp. 145–159, International Press, 1997.

[16] Zeraoulia Rafik and Humberto Salas. Chaotic dynamics and zero distribution: implications and applications in control theory for Yitang Zhang's Landau Siegel zero theorem. *European Physical Journal Plus*, vol. 139, p. 217, 2024. DOI: https://doi.org/10.1140/epjp/s13360-024-05000-w.

[17] A. M. Odlyzko. On the distribution of spacings between zeros of the zeta function. *Mathematics of Computation*, vol. 48, pp. 273–308, 1987.

[18] C. A. Tracy and H. Widom. The Distributions of Random Matrix Theory and their Applications. In: Sidoravičius, V. (ed.) *New Trends in Mathematical Physics*. Springer, Dordrecht, 2009. DOI: 10.1007/978-90-481-2810-5_48.

[19] P. S. Maybeck. Stochastic processes and linear dynamic system models. In: *Mathematics in Science and Engineering*, vol. 141, Part 1, Elsevier, 1979, pp. 133-202. DOI: 10.1016/S0076-5392(08)62169-4.

[20] M. Bourguignon and R. M. R. de Medeiros. A simple and useful regression model for fitting count data. *TEST*, vol. 31, pp. 790–827, 2022. DOI: 10.1007/s11749-022-00801-6.

[21] Alvaro H. Salas and Jairo E. Castillo H. Exact solution to Duffing equation and the pendulum equation. *Applied Mathematical Sciences*, vol. 8, no. 176, 2014, pp. 8781-8789. DOI: 10.12988/ams.2014.44243. Available at: https://hal.archives-ouvertes.fr/hal-01356787.

[22] Nicolas Lanchier. *Stochastic Modeling*. Universitext. Springer Cham, 2016. DOI: https://doi.org/10.1007/978-3-319-50038-6.

[23] Tao, T. (2023). Bounding sums or integrals of non-negative quantities. *WordPress Blog*. Retrieved from https://terrytao.wordpress.com/2023/09/30/bounding-sums-or-integrals-of-non-negative-quantities/

[24] Salas, A. H., & Castillo, J. E. (2014). Exact solution to Duffing equation and the pendulum equation. *Applied Mathematical Sciences*, 8(176), 8781-8789. https://doi.org/10.12988/ams.2014.44243

[25] Wang, P., Yin, F., Rahman, M. U., Khan, M. A., & Baleanu, D. (2024). Unveiling complexity: Exploring chaos and solitons in modified nonlinear Schrödinger equation. *Results in Physics*, 56, 107268. https://doi.org/10.1016/j.rinp.2023.107268

[26] William H. Greene, *A Gamma-distributed stochastic frontier model*, *Journal of Econometrics*, **46**(1–2), 1990, Pages 141-163, ISSN 0304-4076, https://doi.org/10.1016/0304-4076(90)90052-U, https://www.sciencedirect.com/science/article/pii/030440769090052U.

[27] Yochay Jerby, *An approximate functional equation for the Riemann zeta function with exponentially decaying error*, *Journal of Approximation Theory*, **265**, 2021, 105551, ISSN 0021-9045, https://doi.org/10.1016/j.jat.2021.105551, https://www.sciencedirect.com/science/article/pii/S0021904521000149.

[28] Marek Wolf. Will a physicist prove the Riemann Hypothesis? *arXiv preprint arXiv:1410.1214*, 2014. Available at: https://arxiv.org/abs/1410.1214.

[29] James Maynard. Small gaps between primes. *Annals of Mathematics*, vol. 181, no. 1, 2015, pp. 383-413. Available at: https://annals.math.princeton.edu/2015/181-1/p07.